PHYSICAL REVIEW D **82,** 103514 (2010)

# Metastable GeV-scale particles as a solution to the cosmological lithium problem

Maxim Pospelov*
[1]*Department of Physics and Astronomy, University of Victoria, Victoria, BC, V8P 1A1, Canada*
[2]*Perimeter Institute for Theoretical Physics, Waterloo, Ontario N2L 2Y5, Canada*

Josef Pradler†
*Perimeter Institute for Theoretical Physics, Waterloo, Ontario N2L 2Y5, Canada*
(Received 14 July 2010; published 10 November 2010)

The persistent discrepancy between observations of $^7$Li with putative primordial origin and its abundance prediction in big bang nucleosynthesis has become a challenge for the standard cosmological and astrophysical picture. We point out that the decay of GeV-scale metastable particles $X$ may significantly reduce the big bang nucleosynthesis value down to a level at which it is reconciled with observations. The most efficient reduction occurs when the decay happens to charged pions and kaons, followed by their charge-exchange reactions with protons. Similarly, if $X$ decays to muons, secondary electron antineutrinos produce a similar effect. We consider the viability of these mechanisms in different classes of new GeV-scale sectors, and find that several minimal extensions of the standard model with metastable vectors and/or scalar particles are capable of solving the cosmological lithium problem. Such light states can be a key to the explanation of recent cosmic ray anomalies and can be searched for in a variety of high-intensity medium-energy experiments.

DOI: 10.1103/PhysRevD.82.103514 PACS numbers: 98.80.Ft, 12.60.Cn, 14.80.-j, 26.35.+c

## I. INTRODUCTION

Rapid progress in observational cosmology during the last decade brought about the measurements of many cosmological parameters, including a precise determination of the baryon-to-photon ratio $\eta_b$ [1] by the WMAP satellite experiment. This puts the predictions of the big bang nucleosynthesis (BBN) theory on firm footing and allows for less ambiguous comparison with observations. The current status of standard BBN (SBBN) with the input from WMAP can be summarized as follows: there is no dramatic (order of magnitudes) disagreement between predictions and observations, but there is no ideal concordance either. For a series of recent reviews see, e.g., [2–5].

There are at least two quantitative problems that look worrisome: different measurements of the deuterium abundance, although on average consistent with the SBBN prediction, exhibit a significant scatter. This scatter may be the sign of underestimated systematic errors or the manifestation of significant astration, thus hinting on a higher primordial value for the deuterium abundance. In contrast to deuterium, the scatter of $^7$Li/H data points along the so-called Spite plateau [6] is rather small, which for a long time was thought to be a compelling argument for the primordial origin of $^7$Li in these observations. As is well known, this value is a factor of 3–5 lower than the SBBN prediction, $^7\mathrm{Li/H} = (5.24^{+0.71}_{-0.67}) \times 10^{-10}$ [3], which is the essence of the lithium problem.

How serious are these problems of SBBN? It is entirely possible at this point that future higher quality observations of D/H in quasar absorption clouds would render D/H in accordance with SBBN in combination with less scatter. Moreover, more elaborate stellar evolution models with *ab-initio* calculations of lithium diffusion may point to a systematic and uniform reduction of the SBBN value by a factor of 3 or so. At this point, it is too early to declare SBBN being in serious trouble. However, it is also tempting to speculate that some subtle particle-physics interference in the early Universe may have resulted in distorted abundances of the primordial elements, and possibly led to the reduction of lithium abundance.

The primordial value of the lithium abundance is given by the freeze-out BBN value of $^7\mathrm{Be} + {}^7\mathrm{Li}$, with atomic $^7$Be decaying to lithium at the later stages of cosmological evolution. The current lithium problem stems from the overproduction of $^7$Be at $T \sim 40$ keV. $^7$Be cannot be destroyed by protons directly, but instead is depleted via the following chain of exoergic reactions

$$^7\mathrm{Be} + n \rightarrow {}^7\mathrm{Li} \rightarrow {}^4\mathrm{He} + {}^4\mathrm{He}. \tag{1.1}$$

At the second step $^7$Li is destroyed by proton reactions, which remain faster than the Hubble rate until $T \sim 10$ keV.

Different classes of modified BBN models where an additional reduction of lithium can happen were analyzed in the literature over the years. As was first pointed out by Reno and Seckel [7], a (moderate) injection of ''extra neutrons'' around the time of formation of $^7$Li and $^7$Be leads to an overall depletion of $^7\mathrm{Li} + {}^7\mathrm{Be}$ by intensifying the destructive chain (1.1). This was emphasized again after the cosmic microwave background determination of $\eta_b$ in Ref. [8], where it was demonstrated that any particle-physics source is capable of reducing $^7\mathrm{Li} + {}^7\mathrm{Be}$ as long it leads to

*pospelov@uvic.ca
†jpradler@perimeterinstitute.ca

 

the injection of $O(10^{-5})$ neutrons per nucleon at relevant temperatures. Perhaps the most natural source for a neutron excess is the decay of a massive particle species $X$. Independently from the motivation of reducing the $^7$Li abundance, a lot of work has been invested into BBN models with decaying or annihilating particles releasing a significant amount of energy into the primordial plasma [9–15].

So far, most of the analyses have concentrated on the injection of energy by relics with masses comparable to the electroweak scale. This is largely motivated by theoretical arguments in favor of new physics at and below the TeV scale, and by the possibility of having dark matter in the form of weakly interacting massive particles (WIMPs). It can be easily shown that it is unlikely that the residual WIMP annihilation is responsible for the reduction of $^7$Be + $^7$Li, simply because the total energy injected via such mechanism is way below the required levels [7,16]. Known examples that "work," i.e., scenarios in which the $^7$Li abundance is reduced while other elements are still agreeing with observations, typically deal with unstable weak-scale particles. These include some supersymmetric scenarios with the delayed decays of charged sleptons to gravitinos [13,17,18]. The source of extra neutrons in these models is linked to the presence of nucleons among the decay products. An alternative plausible mechanism for reducing $^7$Li is the catalytic suppression of the $^7$Be abundance by the capture of massive negatively charged particles [19–22] that are again linked to the weak scale. In this paper we investigate whether the suppression of the lithium abundance can be triggered by the decays of metastable GeV and sub-GeV scale electrically neutral particles. We address two types of models: the WIMP-type where particle decays were preceded by the depletion through the annihilation, and the super-WIM–type, where the abundance of decaying particles is set by the thermal leakage of standard model (SM) states into an initially vacuous super-WIMP sector.

During the last two years, the GeV-sector phenomenology experienced some degree of revival due to its possible connection to the enhancement of the leptonic fraction of cosmic rays in the pair annihilation of dark matter WIMPs [23,24]. Particularly noteworthy are the enhancement of the positron fraction seen by the PAMELA satellite experiment [25] and the harder-than-expected spectrum for electrons and positrons detected by the Fermi gamma-ray space telescope (FGST) instrument [26]. In such scenarios the GeV-scale particles are designated as "mediators" connecting the dark matter and standard model sectors [27], allowing us to seclude the dark matter by choosing the SM-mediator coupling to be very small, but at the same time keeping the galactic annihilation rate enhanced over the "standard" WIMP scenario.

The motivation for GeV and sub–GeV-scale mediators comes from the following consideration: the lightness of a gauge boson mediating an attractive force in the dark sector, $V(r) = -\alpha_D/r \times \exp(-m_V r)$, compared to the characteristic WIMP momentum inside the galaxy, $m_D v_{\rm gal}$, ensures a Coulomb/Sommerfeld enhancement of the annihilation cross section relative to its freeze-out value. Choosing $m_V \lesssim m_D v \sim 100$ MeV $\div$ 1 GeV, results in a $\pi\alpha_D/v$ enhancement of the cross sections at the relevant velocities. Moreover, once recombination to WIMP-bound states becomes kinematically possible, $m_V < m_D\alpha_D^2/4$, this process dominates numerically over the direct two-body annihilation. The resulting annihilation cross section for fermionic WIMPs can be enhanced over the freeze-out value by 2 to 3 orders of magnitude [24]:

$$\frac{\langle\sigma v\rangle_{\rm gal}}{\langle\sigma v\rangle_{\rm f.o.}} \sim \frac{7\pi\alpha_D}{v_{\rm gal}} \sim O(10^2\text{–}10^3). \tag{1.2}$$

The numerical enhancement due to the bound-state effect over the naive Sommerfeld value is about a factor of 7, accompanied by a possible additional enhancement due to an increased lepton multiplicity in the final state with angular momentum $J = 1$. We note in passing that the important effect of WIMP-onium formation was missed in a recent reanalysis of Ref. [28], that led to the erroneous conclusion that the enhancement factor remains smaller than 100 over the whole parameter space; larger factors were found in [29].

Is it reasonable to expect that the same models that fit the PAMELA and FGST signals [23,24] are also responsible for the suppression of $^7$Li abundance? Even with the inclusion of some very generous enhancement factors, the energy injection during BBN triggered by the annihilation of electroweak-scale WIMPs remains rather small. Moreover, models designed to explain the PAMELA signal tend to minimize the fraction of baryons/antibaryons in the final state [23,24,30,31]. All that, together with previous investigations of BBN with annihilation-induced energy injection, tend to indicate that WIMP annihilation itself cannot be used as a solution to the lithium problem. Therefore, the only chance of altering the BBN predictions for $^7$Be + $^7$Li within this class of models is if the GeV-scale particles from the mediator sector are themselves relatively long-lived, and their decays happen during or after BBN. Interestingly enough, it turns out that the minimal ways of coupling the Standard Model to light mediators often implies the longevity of particles in the GeV sector [32].

The main mechanism by which the decays of the GeV-scale relics in the early Universe can influence the outcome of the BBN is the injection of light mesons such as pions and kaons as well as muons that all lead to the extra source of $p \to n$ conversion. In this work we explore such scenarios, finding the "required" number of injected $\pi^-$, $K^-$, and $\mu^-$ triggering $p \to n$ conversion in the right amount, as well as the "optimal" lifetime-abundance window for such injection. In order to have a consistent cosmological picture, the abundance of parent GeV-scale relics should be small enough so that they carry only a small fraction of the energy density of the Universe during BBN, but still

provide a noticeable number of mesons and muons per nucleon. We show that, in fact, many models with GeV-scale relics fulfill this requirement, including some variants of the models designed to fit PAMELA and FGST signals. We also find that both the WIMP and super-WIMP modifications of a secluded $U(1)_S$ model is capable of reducing the lithium abundance to the observable level.

The structure of this paper is as follows. The next section contains the analysis of the injection of $\pi$, $K$, and $\mu$ particles vs the timing of injection that is needed for reducing $^7$Li. Section III investigates a variety of different models for decaying GeV and sub–GeV-scale relics, and finds the regions of parameter space that lead to the depletion of the lithium abundance. Our conclusions are summarized in Sec. IV. Appendix A contains relevant details with physics input that went into our BBN code.

## II. MESON AND NEUTRINO INJECTION DURING BBN

We begin this section by presenting an overview of the physics processes triggered by the decays of metastable GeV-scale relics $X$ during BBN. Thereby we shall estimate timescales and interaction efficiencies of the crucial reactions which eventually lead to the reduction of the overall $^7$Li BBN prediction. Subsequently, the various final states in the decay of $X$ are considered in detail.

The central parameter entering the discussion is the Hubble expansion rate $H$ as it normalizes any interaction rate during nucleosynthesis. The most relevant epoch for BBN corresponds to the time bracket of 100 sec $\lesssim t \lesssim$ 1000 sec or, equivalently, to a temperature range of

$$1.2 \lesssim T_9 \lesssim 0.4, \tag{2.1}$$

where $T_9$ is the photon temperature in units of $10^9$ K. Thus, in the interesting regime after the annihilation of the electron-positron pairs, the Hubble rate is given by

$$H = \sqrt{\frac{\pi^2 g_{\rm eff}}{90}}\frac{T^2}{M_{\rm P}} \simeq (2.8\times 10^{-3}\ {\rm sec}^{-1})T_9^2 \qquad (T \lesssim m_e), \tag{2.2}$$

where $g_{\rm eff} \simeq 3.36$ counts the radiation degrees of freedom; $M_{\rm P} \simeq 2.43 \times 10^{18}$ GeV is the reduced Planck scale.

The synthesis of $^7$Be, proceeding via $^4{\rm He} + {}^3{\rm He} \to {}^7{\rm Be} + \gamma$, occurs in a more narrow temperature interval, $T_9 \simeq 0.8 \div 0.4$, in which the Hubble rate is $H \sim 10^{-3}$ sec$^{-1}$. This occurs immediately after the opening of the deuterium "bottleneck" at $T_9 \sim 0.8$, when significant quantities of $^4$He and $^3$He are formed, with a helium mass fraction of $Y_p \simeq 0.25$ and a number density of $^3$He per proton of $Y_{^3{\rm He}} \simeq 10^{-5}$. The rate for $^7$Be formation per alpha particle,

$$\Gamma_{^7{\rm Be}} \simeq (10^{-3}\ {\rm sec}^{-1})T_9^{7/3} e^{-12.8/T_9^{1/3}}\left(\frac{Y_{^3{\rm He}}}{10^{-5}}\right) \qquad (T_9 \lesssim 0.8), \tag{2.3}$$

always remains slower than the Hubble rate and quickly becomes completely inefficient due to a strong exponential Coulomb suppression. On the other hand, a nonstandard "thermal" neutron abundance, at the level comparable to $10^{-5}$ has the opportunity to reprocess some fraction of $^7$Be via $^7{\rm Be} + n \to {}^7{\rm Li} + p$ since the rate for a neutron capture per $^7$Be nucleus is

$$\Gamma_{^7{\rm Be}\to{}^7{\rm Li}} \simeq (0.4\ {\rm sec}^{-1})T_9^3\left(\frac{Y_n}{10^{-5}}\right). \tag{2.4}$$

Indeed, looking at the fraction $f_{^7{\rm Be}}$ of $^7$Be which can, in principle, be converted within a Hubble time $\Delta t_H$,

$$f_{^7{\rm Be}} \simeq -\frac{1}{Y_{^7{\rm Be}}}\frac{dY_{^7{\rm Be}}}{dt}\Delta t_H \simeq -H^{-1}\Gamma_{^7{\rm Be}\to{}^7{\rm Li}} \sim -10^7 T_9 Y_n, \tag{2.5}$$

shows that already $Y_n \simeq 5\times 10^{-6}$ at $T_9 \simeq 0.5$ can induce an $\mathcal{O}(1)$ conversion of $^7$Be. $^7$Li in the final state of this reaction is then quickly burned by protons.

The neutron participation in the lithium depleting chain does not influence the abundance of neutrons themselves, because of the small abundance of $^7$Be. Instead, "extra neutrons" are depleted by protons via the $p + n \to {\rm D} + \gamma$ reaction, which, at the relevant temperatures, remains faster than the rate for neutron decay. Comparing the relative changes of $^7$Be and deuterium,

$$\frac{f_{^7{\rm Be}}}{f_{\rm D}} = -\frac{Y_{\rm D}}{Y_p}\frac{\Gamma_{^7{\rm Be}\to{}^7{\rm Li}}}{\Gamma_{p\to{\rm D}}} \sim -10^5({\rm D/H}), \tag{2.6}$$

one can infer that an $\mathcal{O}(1)$ depletion of $^7$Be due to an excess of neutrons will be accompanied by an $\mathcal{O}(1)$ rise in the deuterium abundance since ${\rm D/H} \sim 10^{-5}$. Therefore, the viability of the "extra neutron" solution to the lithium problem should be judged form more accurate quantitative investigations of such scenarios.

The decay of GeV and sub-GeV relic particles with a rate comparable to (2.2) at $T_9 \sim 0.5$ will not lead to a significant population of energetic photons and electrons. The reason for that is well known: very abundant and energetic photons and electrons degrade the energy of the decay products well below the nuclear dissociation thresholds (see, e.g., [10]). Since we explicitly assume the absence of nucleons and antinucleons in the final state, the main effect on the freeze-out abundances of light elements will come from injection of mesons and neutrinos, that are capable of triggering the $p \to n$ conversion and reducing $^7{\rm Li} + {}^7{\rm Be}$. In the following subsections we consider these mechanisms in turn, starting from the simple estimates of the required number of mesons and neutrinos.

### A. Estimates on meson injection

Among the decay products of the GeV-scale metastable states only the long-lived mesons and neutrinos will have a chance to interact with the light elements. Among those,

the most important are charged pions, $\pi^{\pm}$, as well as charged and long-lived kaons, $K^{\pm}$ and $K_L$, respectively. Their masses and lifetimes are given by [33]

$$m_{\pi^{\pm}} = 139.6 \text{ MeV}, \qquad \tau_{\pi^{\pm}} = 2.60 \times 10^{-8} \text{ sec}, \quad (2.7)$$

$$m_{K^{\pm}} = 493.7 \text{ MeV}, \qquad \tau_{K^{\pm}} = 1.24 \times 10^{-8} \text{ sec}, \quad (2.8)$$

$$m_{K^0,\bar{K}^0} = 497.6 \text{ MeV}, \qquad \tau_{K_L} = 5.12 \times 10^{-8} \text{ sec}. \quad (2.9)$$

The decay rate of meson $i$ is related to its lifetime at rest by the familiar time-dilatation formula:

$$\Gamma^i_{\text{dec}} = \left\langle \frac{m_i}{E_i} \right\rangle \frac{1}{\tau_i} \simeq \text{few} \times 10^7 \text{ sec}^{-1}, \quad (2.10)$$

where in the last equality we have taken $\gamma \simeq 1$. More accurately, one has to consider the average value $\langle m_i/E_i \rangle$ over the "lifetime" trajectory of injected mesons. The averaging procedure is significantly different from the usual thermal average when particles obey a Maxwell-Boltzmann distribution. It is determined by the efficiency of various energy degradation mechanisms, of which the most important are Coulomb scattering on electron and positrons and inverse-Compton–type scattering on background photons. Together they determine the thermalization (or stopping) rate $\Gamma^i_{\text{stop}}$. The stopping rate may have a direct impact on the reaction rates with nuclei $\Gamma^i_N$, which are of the primary interest in this paper.

If injected sufficiently early, the charged mesons are effectively stopped within time intervals shorter than their lifetimes $\tau_i$, and before having a chance of participating in a nuclear reaction. The comparison of stopping and decay rate is given by the ratio

$$\frac{\Gamma^i_{\text{stop}}}{\Gamma^i_{\text{dec}}} = \frac{\tau^i_{\text{dec}}}{\tau^i_{\text{stop}}} \simeq \left( \Gamma^i_{\text{dec}} \int_{E_{\text{min}}}^{E_0} \frac{dE}{|dE_i/dt|} \right)^{-1}, \quad (2.11)$$

where $\tau_{\text{stop}}$ measures the energy degradation time from injection energy $E_0$ to some energy $E_{\text{min}}$, below which the kinetic energy of mesons is irrelevant. $dE_i/dt$ represents the energy degradation rate of the particle $i$ traversing the BBN plasma. Requiring complete stopping would correspond to the choice of $E_{\text{min}} \sim 3T/2$, but a more relevant parameter is some characteristic nuclear energy scale. For reactions leading to dissociation of $^4$He, $E_{\text{min}}$ would correspond to $E_{\text{min}} \sim 20$ MeV. In the temperature window (2.1) and for injection energies of $E_0 \lesssim 1$ GeV, Coulomb interactions on $e^{\pm}$ give the dominant contribution to $dE_i/dt$ (for details see, e.g., [10]). Since the number densities of electrons and positrons drop exponentially, the inverse Compton scattering on background photons becomes the dominant energy-loss mechanism for $T < 25$ keV. Taking into account both channels for energy-loss, one typically finds that

$$\frac{\tau^i_{\text{dec}}}{\tau^i_{\text{stop}}} < 1 \quad \text{for } T_9 > (0.3 \div 0.4). \quad (2.12)$$

This point is illustrated in Fig. 1, where the dividing line of "1" separates the two regimes of complete and incomplete stopping. The exponential sensitivity to temperature is reflected in almost vertical contours. Figure 1 tells us that for $t \lesssim 10^3$ sec the charged mesons are thermalized before they decay. Thus, for $i = \pi^{\pm}$ (and analogously for $K^{\pm}$) injected around $T_9 \sim 0.5$ the following hierarchy of scales is applicable:

$$H \ll \Gamma^{\pi}_p \ll \Gamma^{\pi}_{\text{dec}} \lesssim \Gamma^{\pi}_{\text{stop}}. \quad (2.13)$$

The rate for charge-exchange reactions with the most abundant nuclear species, i.e., the rate of proton-to-neutron conversion, is given by

$$\Gamma^{\pi}_p = n_p \langle \sigma v \rangle^{\pi}_{pn} \simeq (3 \times 10^2 \text{ sec}^{-1}) \frac{T_9^3 \langle \sigma v \rangle_{pn}}{1 \text{ mb}}. \quad (2.14)$$

The averaging procedure is again determined along the trajectory of injected mesons and includes both the "in-flight" and "at-rest" contributions. However, for the purpose of a simple estimate, Eq. (2.14) uses the normalization on a typical size of a pion-induced reaction at the threshold. In case of incomplete stopping, this will underestimate the proton-neutron conversion because of the delta-resonance enhancement of the charge-exchange

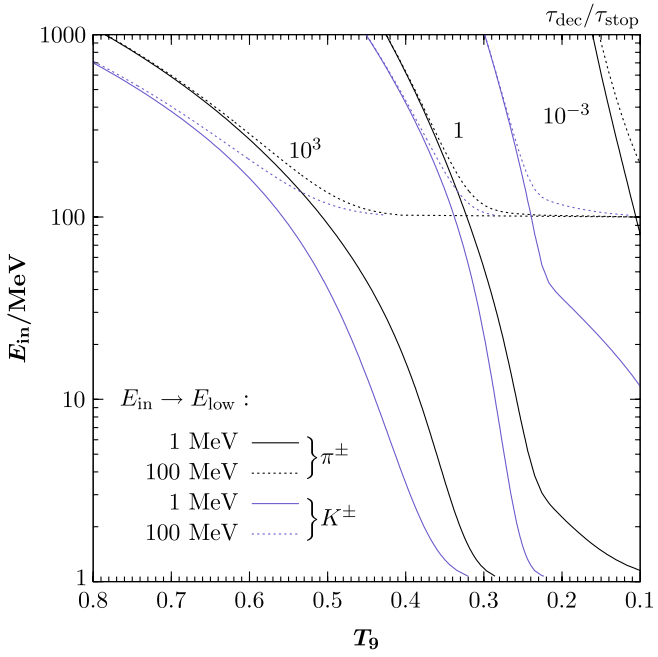


FIG. 1 (color online). Stopping of charged pions and kaons in the plasma as a function of temperature $T_9$, initial injection energy $E_{\text{in}}$, and the minimal energy below which the kinetic energy of mesons can be neglected, $E_{\text{low}}$. The contour $\tau_{\text{dec}}/\tau_{\text{stop}} = 1$ is the dividing line between efficient (left) and incomplete (right) stopping.

reaction. Equation (2.14) immediately leads us to the probability of a charge-exchange reaction of a stopped pion (kaon) on protons during the meson lifetime, per each injected $\pi^-(K^-)$ at $T_9 \sim 0.5$:

$$P^{\pi}_{p\to n} = \int_{t_{\rm inj}}^{\infty} \exp(-\Gamma_{\rm dec}(t - t_{\rm inj}))\Gamma_p dt \simeq \Gamma^{\pi}_p \tau_{\pi^\pm} \sim O(10^{-6}). \quad (2.15)$$

Since every charge-exchange reaction leads to the creation of an extra neutron, the estimate (2.15) represents the *efficiency* of producing neutrons from negatively charged kaons and pions. Notwithstanding the rather crude nature of this estimate, the probability (2.15) tells us that an injection of $\mathcal{O}(10)$ negatively charged pions per proton should be equivalent to the injection of $\mathcal{O}(10^{-5})$ extra neutrons, and thus capable of reducing the overall $^7$Li + $^7$Be abundance by an $\mathcal{O}(1)$ factor.

Since for kaons the charge-exchange cross sections are even higher [7], one can achieve an adequate suppression of $^7$Li + $^7$Be even with the injection of one $K^-$ per baryon. The case of $X$-decays into neutral kaons is special with respect to other meson final states in the sense that $K_L$ has a relatively long lifetime (2.9) but, unlike $\pi^\pm$ or $K^\pm$, is not stopped by electromagnetic interactions. From the conservation of isospin and from the charge independence of strong interactions, we nevertheless expect the impact of $K_L$ on the BBN predictions to be similar to that of $K^-$.

In our treatment, the extra meson species are included in the set of Boltzmann equations, along with the population of parent particles $X$ that decay into mesons and have an abundance with the simple exponential time dependence,

$$Y_X(t) = Y^0_X \exp(-t/\tau_X), \quad (2.16)$$

with $\tau_X$ being the $X$ lifetime. We choose to normalize the $X$ abundance on the total number of baryons, $Y_X \equiv n_X/n_b$; in the following we shall often drop the superscript on $Y^0_X$ for simplicity. When the fast stopping of charged particles is operative at early times, the amount of the injected energy and therefore the actual mass of the $X$ relic are not entering the problem (with $X \to K^0\bar{K}^0$ being the exception.) For later times, the incomplete stopping brings the dependence on the injected energy. We write the Boltzmann equation for meson species $i$ in the following form:

$$\frac{dY_i}{dt} \simeq \sum_j \xi^{(j)}_i Y_j \Gamma^j_{\rm inj} - Y_i \Gamma^i_{\rm dec} - Y_N \Gamma^i_N, \quad (2.17)$$

where $\Gamma^j_{\rm inj}$ is the rate of $i$ injection from source $j$ with multiplicity $\xi^{(j)}_i$. When considering only the primary meson production from $X$ decays such as in the case of $K^\pm$, $\sum_j \Gamma^j_{\rm inj} \simeq \Gamma^X_{\rm dec} = 1/\tau_X$. Given the hierarchy of interactions (2.13), the last term in (2.17) is small. Both $\Gamma^i_{\rm dec}$ and $\Gamma^i_N$ include the effects of incomplete stopping that depends on the initial energy injection $E_0$ and background temperature at the time of injection,

$$\Gamma^i_{\rm dec} = \Gamma^i_{\rm dec}(E_0, T); \qquad \Gamma^i_N = \Gamma^i_N(E_0, T). \quad (2.18)$$

Neglecting subtleties of incomplete stopping at this point, one can find an approximate solution to the Boltzmann equation for mesons in the quasistatic equilibrium approximation $dY^{\rm qse}_i/dt = 0$,

$$Y^{\rm qse}_i = \sum_j \xi^{(j)}_i Y_j \Gamma^j_{\rm inj}/\Gamma^i_{\rm dec} \sim \mathcal{O}(10^{-10}) \times Y_X, \quad (2.19)$$

where in the second relation we assumed multiplicities to be order one, and took $\Gamma_{\rm inj} \sim 10^{-3}$ sec. Even though the equilibrium values for the meson abundances remain low at all times, the $p \to n$ conversion rate for $Y_X \sim \mathcal{O}(10)$ is only 5 orders of magnitude slower than the Hubble rate, thus causing $\mathcal{O}(10^{-5})$ protons be converted to neutrons within one Hubble time. This is consistent with our estimate of efficiency (2.15).

Finally, the pion(kaon)-induced transitions $^7$Be $\to$ $^7$Li and $^3$He $\to$ T also lead to the depletion of $^7$Be. However, these processes are far less important compared to $p \to n$ interconversion. If we assume a fractional $O(10^{-5})$ conversion of $p \to n$ due to $\pi^-$ charge exchange, a similar figure would stand for the $^7$Be $\to$ $^7$Li and $^3$He $\to$ T conversion probabilities, which is completely negligible in the final lithium abundance.

### B. Estimates on muon and neutrino injection

In order to account for the injection of muons and neutrinos one has to deal with quite different physics. The charge-exchange reactions of muons on nucleons are mediated by weak interactions and can be neglected during the muon lifetime of two microseconds. However, the decays of muons, $\mu^- \to \nu_\mu \bar{\nu}_e e^-$, source energetic electron antineutrinos $\bar{\nu}_e$, that survive for a long time, which increases their probability of charge-exchange interaction with protons.

To make our discussion more concrete, we shall assume that all neutrinos originate from muons decaying at rest so that $E_\nu < m_\mu/2$. In this case, the relation between the relevant rates is quite different from (2.13):

$$\Gamma^\nu_p, \Gamma^\nu_{\rm stop} \ll H, \quad (2.20)$$

where $\Gamma^\nu_{\rm stop}$ is the rate of antineutrino energy degradation due to scattering on background neutrinos and electron-positron pairs. This rate scales with temperature and the energy of nonthermal neutrinos $E_\nu(T)$ injected at $T_{\rm inj}$ as follows:

$$\Gamma^\nu_{\rm stop} \sim G_F^2 E_\nu(T) T^4 \sim G_F^2 T^5 \frac{\langle E_\nu(T_{\rm inj})\rangle}{T_{\rm inj}}, \quad (2.21)$$

where we disregard the difference between neutrino and photon temperatures. It is indeed much smaller than the Hubble expansion rate,

$$\frac{\Gamma^{\nu}_{\rm stop}}{H} \sim \left(\frac{T}{3\ {\rm MeV}}\right)^3 \frac{\langle E_\nu(T_{\rm inj})\rangle}{T_{\rm inj}} \sim 10^{-3} \qquad (T, T_{\rm inj} \sim 30\ {\rm keV}), \tag{2.22}$$

where the 3 MeV scale enters as the decoupling temperature of background neutrinos, and the energy of nonthermal antineutrinos is taken to be the average energy in the muon decay, $\langle E_\nu(T_{\rm inj})\rangle = \frac{3}{10} m_\mu \simeq 32$ MeV.

The charged current rate for antineutrino interactions with protons is given by

$$\Gamma^{\nu}_{p} = n_p \sigma^{\bar\nu}_{pn} \simeq 10^{-41}\ {\rm cm}^2 \times \frac{n_p E_\nu^2}{(10\ {\rm MeV})^2} \simeq (3.6\times 10^{-12}\ {\rm sec}^{-1}) \times \frac{T_9^3 E_\nu^2}{(10\ {\rm MeV})^2}, \tag{2.23}$$

where $E_\nu \gg m_e$ is assumed. The ratio of $\Gamma^\nu_p$ to the Hubble rate gives the efficiency of producing extra neutrons from each neutrino injected with $\mathcal{O}(30$ MeV) energy:

$$P^{\nu}_{p\to n} = \int_{t_{\rm inj}}^{\infty} \Gamma^{\nu}_p dt = \frac{1}{3}\frac{\Gamma^\nu_p(T_{\rm inj})}{H(T_{\rm inj})} \sim 2\times 10^{-9}. \tag{2.24}$$

This efficiency is several orders of magnitude smaller than Eq. (2.15), and we conclude that $\mathcal{O}(10^4)$ muon decays per proton are required around $T_9 \sim 0.5$ in order to produce $\mathcal{O}(10^{-5})$ extra neutrons. At the same time, $P^\nu_{p\to n} \ll P^\pi_{p\to n}$ introduces a natural simplification to the problem, as the effects of secondary neutrinos originating from pion and kaon decays can be ignored relative to the direct influence of $\pi^-$ and $K^-$ via the charge-exchange reactions. Moreover, as the efficiency (2.24) also suggests, a direct nuclear-chemical impact of electron antineutrinos on the lithium abundance via $^7{\rm Be} + \bar\nu_e \to {}^7{\rm Li} + e^+$ ($Q = -0.16$ MeV) is negligible.

Having checked that the efficiency of neutron production from pions, kaons, and muons (neutrinos) can be sufficient for the resolution of the lithium problem, we now turn to more detailed calculations. In this regard we would like to emphasize that in what follows we go well beyond the simple estimates presented in the last two sections so that we do not make direct use of (2.15) and (2.24). Some further details on the Boltzmann code that we use can be found in the Appendix.

### C. Decays to pions

Charged pions are a likely final state for almost any hadronic final decay mode. For example, even if $X$ would exclusively decay into $K^\pm$, i.e., $\xi^{(X)}_{\pi^\pm} = 0$ in Eq. (2.17), pions would still be populated by subsequent $K^\pm$ decays, $Y_{K^\pm} \simeq Y_{\pi^\pm}$, since $\xi^{(K^\pm)}_{\pi^\pm} = \mathcal{O}(1)$.

Charged pions have a chance to interact with protons and $^4$He before decaying. Fully thermalized pions have the following charge-exchange reactions on nucleons with positive energy release:

$$\pi^- + p \to n + \gamma{\rm :}\ (\sigma v)^{\pi^-}_{pn(\gamma)} \simeq 0.57\ {\rm mb}, \qquad Q = 138.3\ {\rm MeV}, \tag{2.25}$$

$$\pi^- + p \to n + \pi^0{\rm :}\ (\sigma v)^{\pi^-}_{pn(\pi^0)} \simeq 0.88\ {\rm mb}, \qquad Q = 3.3\ {\rm MeV}, \tag{2.26}$$

$$\pi^+ + n \to p + \pi^0{\rm :}\ (\sigma v)^{\pi^-}_{np} \simeq 1.7\ {\rm mb}, \qquad Q = 5.9\ {\rm MeV}. \tag{2.27}$$

These reactions interconvert neutrons and protons and thereby increase the $n/p$ ratio, because protons are far more numerous once neutrons have been incorporated into $^4$He. The threshold value for the $\pi^- + p$ reaction cross section can be extracted from the lifetime of the pionic hydrogen atom (see, e.g., the review [34]). The strength of the channels $\pi^0$ and $\gamma$ at the threshold can be inferred from the Panofsky ratio [35]. Our value at the (thermal) threshold

$$(\sigma v)^{\pi^-}_{\rm th} \equiv F_{p\pi^-}[(\sigma v)^{\pi^-}_{pn(\gamma)} + (\sigma v)^{\pi^-}_{pn(\pi^0)}] \simeq F_{p\pi^-} \times 1.45\ {\rm mb}, \tag{2.28}$$

is in good agreement with the one used in the BBN literature [7] from where we also took the cross section for $\pi^+ + n$. This threshold value is subject to the usual Coulomb enhancement that is accounted for with the multiplicative factor $F_{p\pi^-}$ in (2.28). For the negatively charged pions and at the temperature range of interest ($T_9 \sim 0.5$) this translates into an enhancement of the reactions rates by a factor of $F_{p\pi^-} \simeq 2$. Further details on Coulomb enhancement are provided in the Appendix A 1.

The incomplete stopping of pions introduces an important modification to the rates of these reactions, and to the efficiency of $p \to n$ conversion. To quantify this effect, we introduce the correction factor $\kappa(E_0, T)$ as a function of primary kinetic injection energy $E_0$ that includes both the effect of the time dilatation (and effectively longer lifetimes of fast pions) and, more importantly, the momentum dependence of the cross section that has a strong peak around a pion energy of $E_\pi \sim 180$ MeV:

$$\kappa(E_0, T) \equiv \frac{P_{p\to n}(E_0, T)}{P_{p\to n}(T)} = \frac{1}{\tau_\pi (\sigma v)_{\rm th}} \int_0^\infty dt (\sigma v)_{E_\pi(t)} \times \exp\left(-\int_0^t dt' \frac{1}{\tau_\pi \gamma(E_\pi(t'))}\right). \tag{2.29}$$

The exponential factor in this expression is the survival probability, that is the probability of finding a meson at time $t$ after its injection at $t = 0$. Defined this way, the correction factor $\kappa(E_0, T) = 1$ in the limit of $\tau_{\rm stop} \ll \tau_\pi$. Notice also that due to the scale hierarchy, $H \ll \tau_\pi^{-1}$, we can disregard the effects related to the cosmological

expansion inside the integrals of Eq. (2.29), and set the initial moment of injection to be $t = 0$.

The kinetic energy $E_\pi$ of an injected pion, and the time $t$ along the lifetime trajectory are related via the rate of energy loss:

$$t(E_\pi) = \int_{E_\pi}^{E_0} \frac{dE'}{|dE'/dt|}; \qquad \frac{dE}{dt} = \left(\frac{dE}{dt}\right)_{\rm Coul} + \left(\frac{dE}{dt}\right)_{\rm Comp}. \tag{2.30}$$

As alluded before, $dE/dt$ is a strong function of the background temperature. Finding the explicit dependence between time and kinetic energy of injected pions numerically, and using the experimental data for the inelastic $p + \pi^-$ reaction away from threshold, we find the correction factor for the efficiency, $\kappa(E_0, T)$. Figures 2 and 3 plot this factor for the representative temperature and initial energy slices. One can see that due to incomplete stopping at late times, the correction factor can be very large, possibly reaching

$$\kappa_{\rm max} \simeq \gamma_{\rm max} \frac{(\sigma v)_{\rm max}}{(\sigma v)_{\rm th}} \simeq 30, \tag{2.31}$$

where $\gamma_{\rm max} \simeq 2.3$ corresponds to the pion momentum at delta resonance, where the ratio of cross sections reaches $(\sigma v)_{\rm max}/(\sigma v)_{\rm th} \simeq 14$.

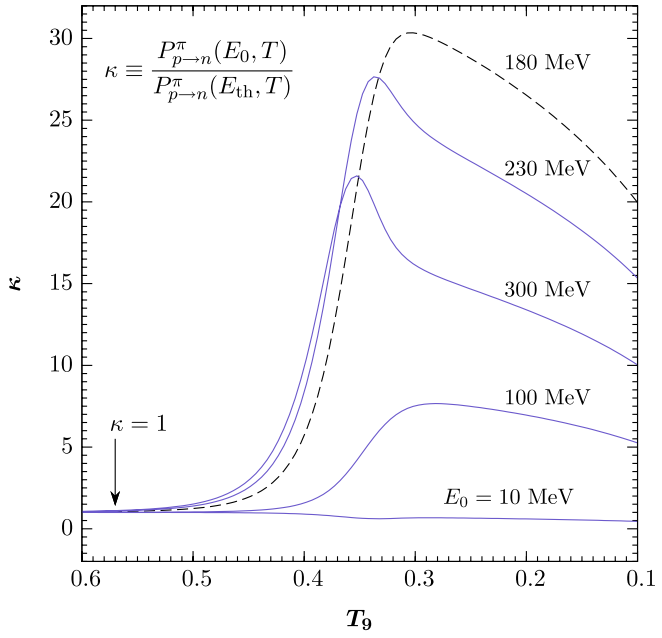


FIG. 2 (color online). The correction factor $\kappa(E_0, T)$, relating the efficiency of $p \to n$ conversion by pions in flight to the thermal case, as a function of temperature for representative values of injection energy $E_0$; $E_{\rm th} = 3T/2$. The dashed line shows the case of maximal efficiency due to pion injection at the delta-resonance energy. Formally, $\kappa < 1$ is possible for low temperatures and small injection energies because the Coulomb corrections of a fully thermalized pion are substantial.

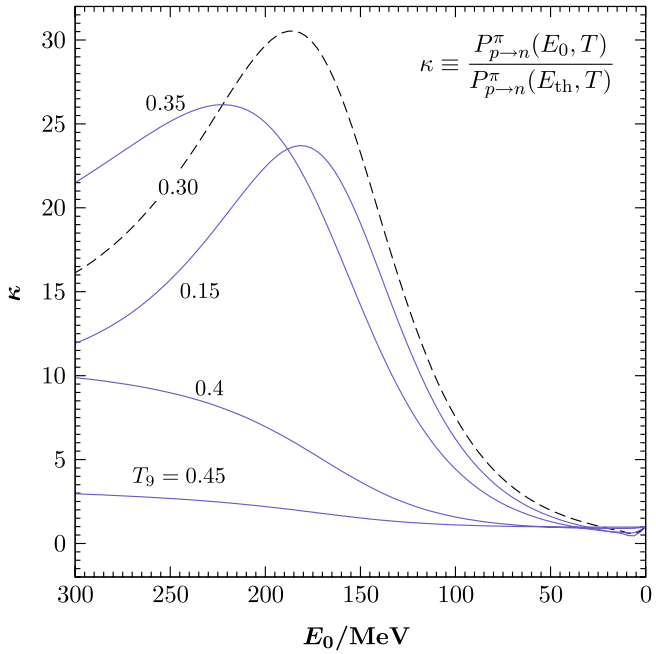


FIG. 3 (color online). The correction factor $\kappa(E_0, T)$, relating the efficiency of $p \to n$ conversion by pions in flight to the thermal case, as a function of injection energy $E_0$ for representative values of temperature. The curves corresponding to late injection $T_9 = 0.15$ and 0.3 when stopping does not occur follow the familiar energy-dependent profile of the pion-nucleon cross section with the broad delta resonance at 180 MeV.

At the next step we account for the possible reactions on $^4$He. Again, we separate our discussion into the reactions induced by stopped and in-flight pions. Charge-exchange reactions of thermal $\pi^\pm$ on $^4$He are not possible because of the deep binding of $^4$He compared to other mass-4 isomers. However, $\pi^\pm$ can be fully absorbed by $^4$He leading to a $\sim$100 MeV energy release and a variety of nuclear final states. Moreover, the reactions with thermal $\pi^+$ are suppressed because of the Coulomb repulsion, and thus we concentrate on $\pi^-$ absorption. A measurement of the ground state level width $\Gamma_{1S} = (45 \pm 3)$ eV [36] of pionic helium then allows us to obtain the total low-energy in-flight cross section $(\sigma v) \simeq 7.3$ mb; for further details see Appendix A 2. The branching ratios into the different final states have been measured [37] to be (T$n$):(D$nn$):($pnnn$) = $(17 \pm 9)$%:$(63 \pm 26)$%:$(21 \pm 16)$%. Adopting the central values (with 20%$pnnn$) we arrive at

$$\pi^- + {}^4{\rm He} \to {\rm T} + n{:}\ (\sigma v)^{\pi^-}_{{\rm T}n} \simeq 1.1\ {\rm mb}, \qquad Q = 118.5\ {\rm MeV}, \tag{2.32}$$

$$\pi^- + {}^4{\rm He} \to {\rm D} + 2n{:}\ (\sigma v)^{\pi^-}_{{\rm D}nn} \simeq 4.1\ {\rm mb}, \qquad Q = 112.2\ {\rm MeV}, \tag{2.33}$$

$$\pi^- + {}^4{\rm He} \to p + 3n{:}\ (\sigma v)^{\pi^-}_{pnnn} \simeq 1.3\ {\rm mb}, \qquad Q = 110\ {\rm MeV}. \tag{2.34}$$

Before using (2.32) in our code, we account for Coulomb corrections, which leads to the enhancement of $F_{^4\mathrm{He}\pi^-} \simeq 3.5$.

The reactions of "in-flight" pions with $^4$He can also be significantly enhanced by the presence of the delta resonance. Again, one has to distinguish two types of reactions, inelastic scattering, $\pi^\pm + {}^4\mathrm{He} \to \pi + N$, and absorption, $\pi^\pm + {}^4\mathrm{He} \to N$ where $N$ represents a variety of multinucleon/nuclear final states. We use the results of experimental studies [38–40] to account for the pion-$^4$He reactions across the delta resonances. We also extrapolate these results to the threshold regions, and calculate effective cross sections to the various (exclusive) final states by averaging over the pion lifetime trajectory while taking into account the respective energy-dependent branchings. The details of this procedure are summarized in Appendix A 3.

Besides enhancing the number of free neutrons, the reactions on $^4$He have an additional important effect: they produce energetic $A = 3$ elements that are able to participate in the nonthermal reactions leading to $^6$Li. For example, reactions with thermalized $\pi^-$ in Eq. (2.32) in $\sim$17% of all cases contain T nuclei with an energy $E_{\mathrm{T}}^{\mathrm{in}} \simeq 30$ MeV injected into the plasma. This leads to a possible secondary source of $^6$Li via their fusion on ambient alpha particles [7,41],

$$\mathrm{T} + {}^4\mathrm{He}|_{\mathrm{bg}} \to {}^6\mathrm{Li} + n \quad Q = -4.8\ \mathrm{MeV}. \tag{2.35}$$

The number of produced $^6$Li per injected T (and likewise per injected $^3$He) can be found by tracking the T degradation from $E_{\mathrm{T,in}}$ until the threshold energy in the frame of the thermal bath, $E^{\mathrm{T}}_{^6\mathrm{Li,th}} \simeq 8.4$ MeV,

$$N_{^6\mathrm{Li}} \simeq \int_{E^{\mathrm{T}}_{^6\mathrm{Li,th}}}^{E_{\mathrm{T,in}}} dE_{\mathrm{T}} \frac{n_{^4\mathrm{He}} \sigma_{\mathrm{T}(^4\mathrm{He},n)^6\mathrm{Li}} v_{\mathrm{T}}}{|dE_{\mathrm{T}}/dt|}, \tag{2.36}$$

where $v_T$ is the velocity of T. As is well known, the production of $^6$Li becomes more efficient at late times, when its thermal destruction slows down. This occurs in the regime of $\tau_\pi \ll \tau_{\mathrm{stop}}$, and most of the energetic $A = 3$ elements originate from $^4$He reacting with in-flight $\pi^\pm$. This complicates the treatment of finding the final $^6$Li abundance as the branching to $A = 3$ elements become energy dependent. Moreover, nonabsorptive inelastic pion-helium reactions result in mass-3 injection spectra which are continuously distributed. We account for all these effects with details presented in Appendix A 3.

In a final step we also account for potential effects on the light element abundances coming from the "visible" energy injection in the decays of the pions. Any primary electromagnetic energy deposition $E_{\mathrm{inj}}$ is quickly dispersed in an electromagnetic cascade with $E_{\mathrm{inj}}$ shared among a large number of photons. Photons with energies less than $E_C \simeq m_e^2/22\mathrm{T}$ [42] lose their ability to pair create $e^\pm$ in scatterings on the background radiation. Those associated "breakout" photons can then destroy the light elements. The earliest time at which this happens can be determined by equating $E_C$ to the nuclear binding energies $E_b$ against photodissociation:

$$t_{\mathrm{ph}} \simeq \begin{cases} 2 \times 10^4\ \mathrm{sec} & \text{for } {}^7\mathrm{Be} + \gamma \to {}^3\mathrm{He} + {}^4\mathrm{He} \quad (E_b = 1.59\ \mathrm{MeV}) \\ 5 \times 10^4\ \mathrm{sec} & \text{for } \mathrm{D} + \gamma \to n + p \quad\quad\quad\quad\ (E_b = 2.22\ \mathrm{MeV}) \end{cases}.$$

We see that the electromagnetic energy injection plays no role in the most interesting $X$-lifetime region $\tau_X \lesssim 10^4$ sec in which the lithium depleting chain (1.1) is operative. Only for $\tau_X > 10^4$ sec do we expect an influence on the element abundances, starting with the destruction of $^7$Be followed by D. The deepest bound element, $^4$He is only destroyed for $t > 10^6$ sec. Charged pions decay into $\mu^\pm$ which are, however, not initiating an electromagnetic cascade since for $t \gtrsim 10^4$ sec their rate for Thomson scattering becomes smaller than the muon decay rate. Thus, for simplicity, we assume that a total of $E_{\mathrm{inj}} = \langle E_e \rangle = (7/20) m_\mu$ per $\pi^\pm$ is injected in the form of electromagnetic energy, where $\langle E_e \rangle$ is the average electron energy in the muon decay. Fortunately, though this neglects a certain fraction of accessible kinetic energy of the muon, a more accurate treatment is inconsequential for our further discussion. On the same footing, we also neglect a direct energy production in $X$ decay via, e.g., $X \to \pi^0 \pi^0$. More details can be found in Appendix A 4.

The pion-enriched BBN was run for different input values of $\xi^{(X)}_{\pi^\pm} Y^0_X$, $\tau_X$ and the pion injection energy $E_0$. In Fig. 4 we plot an example of one possible choice with $Y^0_X = 8$, $\xi^{(X)}_{\pi^\pm} = 1$, $\tau_X = 10^3$ sec and negligible kinetic energy of injected pions. As expected, one can see a noticeable increase of neutrons at lithium-relevant temperatures. This leads to a decrease in the $^7$Be abundance and also an increase in D/H. The secondary source of $^6$Li although leading to a modest increase of $^6$Li over the SBBN prediction, turns out to be far below the observable level of $^6\mathrm{Li/H} \sim 10^{-11}$. This is because the $^6$Li-burning reactions are very fast above $T_9 > 0.1$.

The exploration of the full parameter space yields the region in which the primordial lithium overproduction problem is solved. For this solution, we require $^7$Li/H to stay in the interval

$$^7\mathrm{Li/H} = (1 \div 2.5) \times 10^{-10}. \tag{2.37}$$

The ballpark of observations lie in the range $\sim 1.5 \div 2.0$ (see, e.g., [2,4] and references therein), but also values on

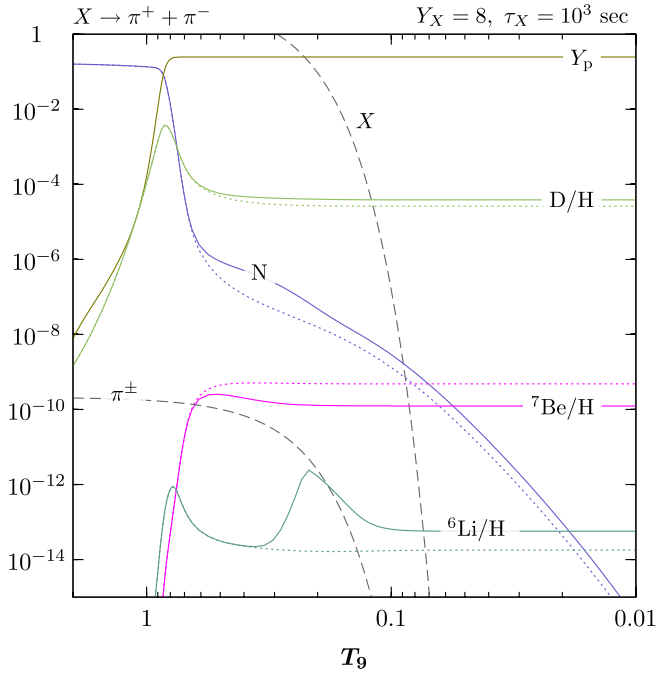


FIG. 4 (color online). Temperature evolution of light nuclei, metastable parent $X$ particles and daughter $\pi^\pm$ mesons for $Y_X = 8$ and $\tau_X = 10^3$ sec as input values and for the injection not too far from threshold. The pion-induced elevation of $n/p$ around $T_9 \sim 0.5$ leads to the expected increase in the D/H and $^6$Li/H abundances, and to a decrease in $^7$Be/H when compared with the respective SBBN predictions (dotted lines); $N$ is the neutron abundance normalized to baryons.

the upper end of the adopted range have been reported [43,44]. For completeness, we also mention that the latest observations seem to suggest what could be called a drop-off of stars from the most metal-poor end of the Spite plateau [45,46] (toward lower values of $^7$Li/H.) It is important to note that such a feature, as puzzling as it may be, in itself does not alleviate the tension between the SBBN prediction and the lithium observations, but rather enhances the controversy. The observational status on that issue is still very much under dispute, as is best illustrated recently by Ref. [47]. That work does not seem to confirm such a "sagging tail" in $^7$Li/H but rather finds two plateau values, $\sim$1.5 and $1.9 \times 10^{-10}$. At this point, we choose the range (2.37) based on the overall range of lithium abundance in the metal-poor stars along the Spite plateau. Should the mechanisms for astrophysical depletion of the lithium abundance firm up, the range (2.37) must be shifted upward.

In addition to (2.37), we shall also put the following constraints on the remaining light elements which are produced in observable quantities in BBN:

$$\mathrm{D/H} \leq 4 \times 10^{-5}, \tag{2.38}$$

$$0.24 \leq Y_p \leq 0.26, \tag{2.39}$$

$$^6\mathrm{Li/H} \leq 6 \times 10^{-11}, \tag{2.40}$$

$$^3\mathrm{He/D} \leq 1. \tag{2.41}$$

The upper limit (2.38) corresponds to the highest reliable determination [48,49] of D/H in a QSO absorption system with a simple enough velocity structure. Given the significant scatter in the various determinations of its primordial value, the possibility of deuterium astration remains and values as high as (2.38) cannot be convincingly excluded at the present stage. For $^4$He the inference of its primordial mass fraction is potentially plagued by systematic uncertainties and values in the range (2.39) have been witnessed over the years with most recent determinations being on the higher side [50,51]. Observations of the isotopic ratio $^6$Li/$^7$Li in metal-poor halo stars are extremely difficult. Though a 5% plateau value has been claimed [52], its inference has also been challenged [53] so that we only impose (2.40) as an upper limit. Finally, D being more fragile than $^3$He, the ratio $^3$He/D is a monotonically increasing function of time so that the solar-system value (2.41) [54] provides an upper limit on the primordial value.

In Fig. 5 we present a parameter scan in the $(\tau_X, \xi_\pi^{(X)} Y_X)$ plane with $\xi_\pi^{(X)} = 1$, with the assumption of negligible kinetic energy of injected pions, so that all reactions and decays occur at rest. The star is the point in parameter space for which Fig. 4 was obtained. The shaded band shows the region in which $^7$Li/H is within the observationally favored range (2.37). More pions become available for larger values of $Y_X$ so that $(^7\mathrm{Li} + {}^7\mathrm{Be})/\mathrm{H}$ decreases from its SBBN value $\sim 5 \times 10^{-10}$ at $Y_X = 1$ to $2.5 \times 10^{-10}$ at the lower border of the shaded band. As expected, there is also an associated increase of D/H from its SBBN value, $\sim 2.6 \times 10^{-5}$, with contours of constant deuterium shown by the dotted lines and running almost in parallel to constant lithium. The lowest D/H value along the $^7$Li/H band is $3.25 \times 10^{-5}$ (for $\tau_X \leq 10^4$ sec ). The contours of constant $^4$He are shown by the solid lines. The effect on $^4$He becomes stronger for smaller $X$-lifetime values. As is well known, $^4$He exhibits the strongest sensitivity on neutron/proton interconversions which take place before the opening of the deuterium bottleneck. We further observe that the secondary production of $^6$Li (2.32) becomes only important for large lifetimes $\tau_X \gtrsim 10^4$ sec (dashed line). This, however, is already the region in the parameter space in which the proposed mechanism for lithium depletion by extra neutrons becomes inefficient. By the same token, the photo destruction of light elements remains decoupled from the main effect as it only happens at late times (2.37). The destruction of $^7$Be and D can, respectively, be seen by the downward trend of the lithium band as well as by the dotted curve labeled "2." Finally, we note that the ratio (2.41) of $^3$He/D is never saturated throughout the whole $(\tau_X, Y_X)$ plane. The dark (blue) shading of the band corresponds to the region in which all constraints (2.37),

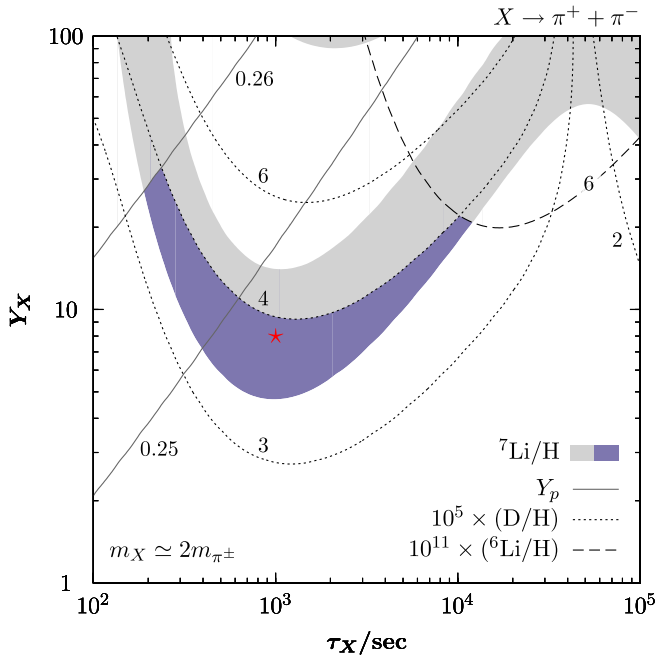


FIG. 5 (color online). Light element abundance yields in the plane of $X$ lifetime vs $X$ abundance (prior to decay), $(\tau_X, \xi_\pi^{(X)} Y_X)$ with $\xi_\pi^{(X)} = 1$ and negligible kinetic energy of injected pions. The band shows the region $10^{-10} \leq {}^7\mathrm{Li/H} \leq 2.5 \times 10^{-10}$ in which the BBN lithium prediction is reconciled with observationally inferred primordial values. In the dark (blue) shaded part all limits (2.38), (2.39), (2.40), and (2.41) on the remaining light elements are respected. Contours of constant helium mass fraction $Y_p$ are shown by solid lines and of constant D/H abundance by dotted lines; the dashed line in the upper right corner corresponds to ${}^6\mathrm{Li/H} = 6 \times 10^{-11}$ with smaller values anywhere below. The star is the point in parameter space for which Fig. 4 was obtained.

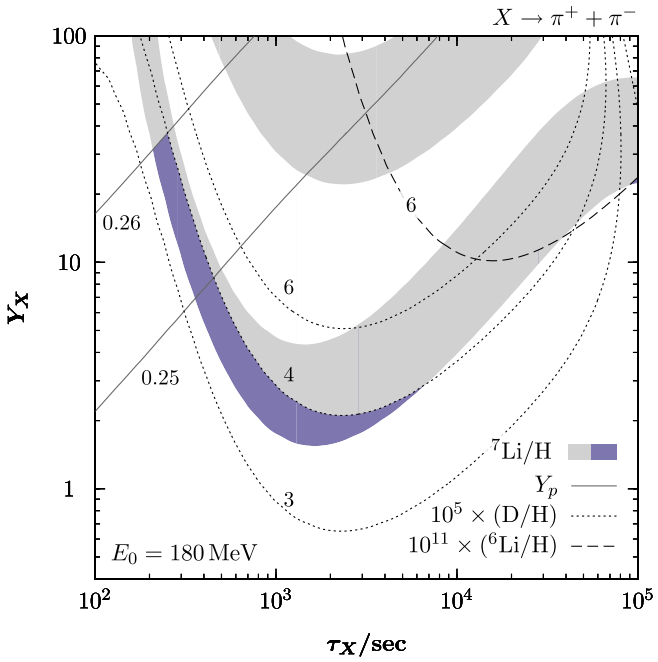


FIG. 6 (color online). Same as in Fig. 5, but with a kinetic energy of injected pions $E_0 = 180$ MeV which approximately corresponds to the maximum of the pion-nucleon cross section.

(2.38), (2.39), (2.40), and (2.41) are obeyed. It is this region, for which the pion injection provides a satisfactory solution to the lithium overabundance problem.

As was argued earlier, pions with kinetic energy close to the delta-resonance may have a considerably larger efficiency of $p \to n$ conversion below $T_9 \simeq 0.4$. To demonstrate this point, we take the same assumptions as in Fig. 5 but assume a primary pion injection energy of $E_0 = 180$ MeV. The results of the new scan are presented in Fig. 6. The increased efficiency of $p \to n$ conversion (along with stronger $\pi^\pm - {}^4$He reactions) leads to a lowering of the bands, i.e., less pions per baryon are necessary for the required depletion of ${}^7$Li. Note, however, that the overall effect is somewhat milder than initially expected. For a lifetime $\tau_X = 10^3$ sec at which pions are still being stopped, one finds a factor $\sim 2 \div 3$ reduction in $Y_X$. For larger lifetimes it only becomes about half an order of magnitude (note the slightly different scales on the y axes of Figs. 5 and 6.) Though ${}^7$Be is indeed efficiently destroyed by strongly elevated neutron concentrations it turns out that the limiting factor is the final step in the overall ${}^7\mathrm{Be} + {}^7\mathrm{Li}$ depleting chain (1.1), i.e., the subsequent ${}^7$Li destruction via thermal proton burning, ${}^7\mathrm{Li} + p \to {}^4\mathrm{He} + {}^4\mathrm{He}$. This latter reaction effectively shuts off for $T_9 < 0.3$ and the overall lithium abundance is produced in the form of ${}^7$Li. Residual late $X$ decays at temperatures $T_9 \lesssim 0.5$ also lead to the narrowing of the lithium band at small lifetimes $\tau_X < 10^3$ sec and large $Y_X$. We remark in passing that in that region, the accompanying increase in D also leads to an enhancement in the $n$-sourcing thermonuclear DD and DT fusion reactions.

### D. Decays to kaons

Aiming at a reasonably accurate treatment of kaons is even more difficult. Let us first focus on $K^\pm$, and assume for simplicity that the kinetic energy is relatively small, so that one can neglect the effects of the decay in flight. In the case of kaon injection it is important to include their hadronic decays into charged pions, as well as the direct interaction of kaons with nucleons. The production of charged pions in kaon decays is relatively easy to account for:

$$K^\pm \to \begin{cases} \pi^\pm \pi^0 (\pi^0) & 22.4\% \\ \pi^\pm \pi^+ \pi^- & 5.6\% \end{cases},$$

which leads to a comparable population of $K^\pm$ and $\pi^\pm$. As has been already mentioned, there is no need to track muons (and the associated neutrino yield) since $P^\nu_{p\to n} \ll P^\pi_{p\to n}$. For the average kinetic energy of produced charged pions we take $E_0 \sim 80$ MeV. Even in the two-body decay,

$\pi^{\pm}$ have energies of only ~110 MeV so that they fall somewhat lower than the $\Delta$ resonance, and their incomplete stopping at late times will not have a large effect on the efficiency of $p \to n$ conversion.

We now turn to the calculations of the direct capture of kaons on nucleons. Whereas the charge-exchange reaction $K^- + p \to \bar{K}^0 + n$ has $Q = -5.2$ MeV and is thus not allowed kinematically on the threshold, $K^-$ reactions on nucleons can proceed via the "$s$-quark exchange reactions" with hyperons and pions in the final state:

$$K^- + p \to \Sigma^{\pm}\pi^{\mp}, \Sigma^0\pi^0, \Lambda\pi^0, \tag{2.42}$$

$$K^- + n \to \Sigma^-\pi^0, \Sigma^0\pi^-, \Lambda\pi^-. \tag{2.43}$$

In order to obtain the inclusive $n \leftrightarrow p$ interconversion cross sections, one then has to take into account the decays of the strange baryons in the final states

$$\Sigma^+ \to \begin{cases} p\pi^0 & 51.6\% \\ n\pi^+ & 48.3\% \end{cases}, \qquad \Lambda \to \begin{cases} p\pi^- & 63.9\% \\ n\pi^0 & 35.8\% \end{cases},$$
$$\Sigma^- \to n\pi^0 \ \ 99.8\%, \qquad \Sigma^0 \to \Lambda\gamma \ \ 100\%. \tag{2.44}$$

The cross section for each of the processes (2.42) and (2.43) and can be obtained in terms of an isospin ($I$) decomposition of the wave functions of the reactants. Together with the knowledge of the relative phases $\phi$ of the individual isospin amplitudes, the cross sections can then be inferred from the total $K^-$-absorption cross sections of a given $I$,

$$\sigma_I \simeq \frac{4\pi b_I}{k}\left|\frac{1}{1 - ikA_I}\right|^2, \tag{2.45}$$

where $A_I = a_I + ib_I$ are complex scattering lengths; $k$ is the c.m. momentum of the incoming state. Taking into account the deviations from charge independence due to $n$, $p$, and $K^{\pm}$ and $K^0$ mass differences following [55,56] and using $A_0 = (-1.74 + i0.70)$ fm, $A_1 = (-0.05 + i0.63)$ fm, $\phi_{\rm th} = -52.9°$ as well as a ratio 0.34 of $\Lambda\pi^0$ to total $I = 1$ hyperon production [56] one arrives at the values for (2.42) and (2.43). In a final step, we use the branching ratios (2.44) to obtain the inclusive threshold cross sections for proton/neutron interconversion,

$$K^- + p \to n + X\text{: } (\sigma v)^{K^-}_{pn} \simeq 32 \text{ mb}, \tag{2.46}$$

$$K^- + n \to p + X\text{: } (\sigma v)^{K^-}_{np} \simeq 13 \text{ mb}, \tag{2.47}$$

where in (2.46) the Coulomb correction has been factored out. Whereas the first cross section is in good agreement with the value previously used in the BBN context, the second one is a factor of 2 smaller than in [7]. In this regard, we remark in passing that the latter reactions (2.43) are only due to $I = 1$ scatterings.

In principle, the nucleons for some of the final states of (2.46) and (2.47) can have energies on the order of 30 MeV. While protons will be stopped before inducing any nuclear changes, neutrons with such energies are stopped primarily via interactions with $p$ and $^4$He, and could split $^4$He nuclei in the collisions into some of its constituents. However, since $^4$He is 1 order of magnitude less abundant than $p$, and since the maximum energy of $n$ is close to the $^4$He desintegration threshold, we neglect such secondary effects. In addition, we further note that due to isospin invariance we do not need to consider hyperon production processes in $K^+n$ scatterings.

As in the case of $\pi^- + {}^4$He, reactions of $K^-$ on helium have not been considered in the BBN context. Fortunately, the measurements of Ref. [57] provide us with a detailed list of branching ratios for $K^-$ absorption on $^4$He at rest. By accounting for the decay modes (2.44) we find the following particle multiplicities per $K^-$ absorption

$$\xi_{^3\rm He} \simeq \xi_{\rm T} \simeq 0.13, \qquad \xi_n = 1.57 - 0.34\lambda_{\rm D},$$
$$\xi_{\rm D} = 0.17 + 0.34\lambda_{\rm D}, \qquad \xi_p = 1.29 - 0.34\lambda_{\rm D}. \tag{2.48}$$

When a final state is not resolved we have, for simplicity, assumed that a fraction of $\lambda_{\rm D}$ is released in the form of D and $(1 - \lambda_{\rm D})$ in the form of nucleons, and we adopt $\lambda_{\rm D} = 0.5$. Thus, for example, in the reaction $K^- + {}^4\text{He} \to \Lambda(\Sigma^0)(pnn)$, which occurs with branching fraction 22.5%, we assume 50% $\Lambda(\Sigma^0)(Dn)$ and 50% $\Lambda(\Sigma^0)(pnn)$. Thereby, we are neglecting a certain fraction of mass-3 nuclei. In this regard, note that—unlike in the case of the threshold reaction $^4\text{He} + \pi^-$—an accurate computation of the secondary $^6$Li yield is more difficult as the $^3$He/T injection energy is now continuous. However, as we have already seen in the previous section, $^6$Li production in excess of observationally constrained levels is an issue only in the region where (1.1) looses its efficiency. Therefore, we shall make the simple assumption that on average T and $^3$He carry one third of the liberated energy, $\langle E_{\rm T}\rangle \sim 30$ MeV and $\langle E_{^3\rm He}\rangle \sim 50$ MeV, respectively. (With our assumptions) the latter value is higher as $^3$He stems predominantly from processes with $\Lambda$ and not $\Sigma$ production. Finally, we note that the contribution of hyperfragments of $^4_\Lambda$He is ~2% [57] which thus does not pose any further complication. With the above multiplicities (2.48) one then obtains effective cross sections for each isotope in the final state,

$$K^- + {}^4\text{He} \to N + \Pi\text{: } (\sigma v)^{K^-}_N = \xi_N(\sigma^{K^-}_{^4\rm He} v), \tag{2.49}$$

with $\Pi$ symbolizing an arbitrary pionic final state and $N = {}^3$He, T, D, $n$, or $p$. The extraction of $(\sigma v)^{K^-}_N$ is similar to the pion case and is given by (A8) in Appendix A 2.

In order to take into account the effects from electromagnetic energy injection in kaon decays we recall from the previous section that $\pi^{\pm}$ as well as $\mu^{\pm}$ are unlikely to initiate an electromagnetic cascade for $\tau_X \gtrsim 10^4$ sec. The multiplicities in the $K^{\pm}$ decay to $\mu^{\pm}$ (including muons from $\pi^{\pm}$ final states) and to $\pi^0$ are $\xi^{K^{\pm}}_{\mu} \simeq 1$ and $\xi^{K^{\pm}}_{\pi^0} \simeq 0.3$, respectively. For the electromagnetic energy release in the

muon decay we again take $E^{\mu}_{\rm inj} \simeq m_{\mu}/3$ and for $\pi^0$ we assume that, in addition to their rest mass, they carry on average approximately one third of the energy released in the particular decay channel, yielding $E^{\pi^0}_{\rm inj} \sim 250$ MeV. Taken together, this amounts to a "branching fraction" $\mathrm{Br}_{K^{\pm}\to\mathrm{vis}} \sim 0.55$ and a total electromagnetic energy injection of $E_{\rm inj} \sim 2 \times \mathrm{Br}_{K^{\pm}\to\mathrm{vis}} m_{K^{\pm}}$ per $X$ decay. As for simplicity we assume that the kaon kinetic energy is small, we do not have to worry about the increase of the electromagentic deposition by decaying in-flight kaons. However, we emphasize that even in the case of slow kaons, and because of the exponential sensitivity to $\tau_X$, $\mathcal{O}(10)$ $K^{\pm}$ per baryon will have a strong effect on nuclear abundances once a photodissociation threshold is met for $\tau_X > 10^4$ sec.

The kaon-induced solution to the cosmological lithium problem is plotted in Fig. 7. In contrast to the case of primary pions at rest (see Fig. 5), a reduction of $^7$Li/H to observed values (2.37) is already possible for one injected kaon per baryon. This is evidently due to the fact that $K^-$ cross sections on nucleons and helium are significantly larger than for thermal $\pi^-$. Moreover, pions from kaon decays only amplify any effect on the light elements. Notice, however, that for too high of an $n$ abundance (large $Y_X$) $^7$Li + $^7$Be starts to increase again. Though $^7$Be is still being depleted, the net production of lithium in form of $^7$Li

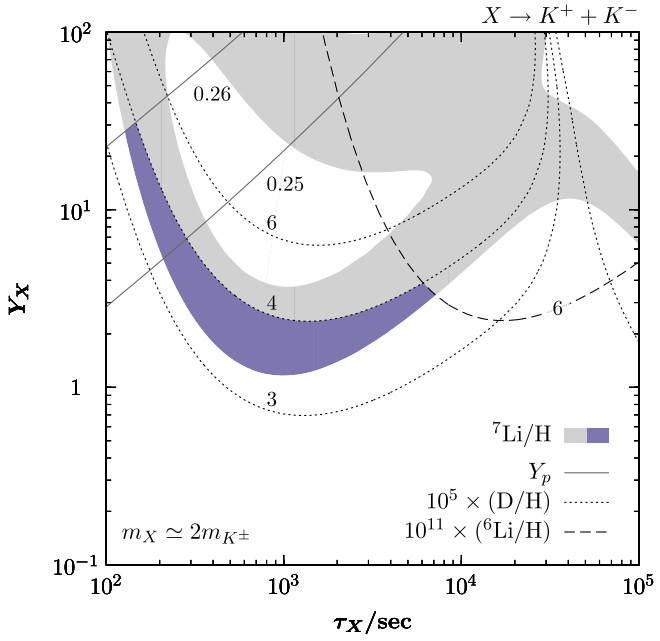


FIG. 7 (color online). Same as in Fig. 5, but for the case of $K^{\pm}$ injection and assuming one charged kaon pair per $X$ decay, $\xi^{(X)}_{K^{\pm}} = 1$, being injected close to the kinematic threshold. Because of the larger cross sections of $K^-$ on nucleons and helium, one requires a fewer number of initial $X$ decays. The trend of depleting $^7$Be + $^7$Li for larger values of $Y_X$ is eventually reverted because of the enhanced production of lithium in form of $^7$Li due to numerous extra neutrons.

eventually takes over. Similar to the case of primary $\pi^{\pm}$ we find that solutions corresponding to $\tau_X \gtrsim 10^4$ sec are not viable because of $^6$Li overproduction. This again excludes the potentially interesting region with $\tau_X = \text{few} \times 10^5$ sec in which previously formed deuterium is destroyed in photodissociation and brought back to its SBBN prediction.

We now turn to the case of injected neutral kaons $K^0$, $\bar{K}^0$—propagating as $K_L$ and $K_S$. Whereas $K_S$ definitely decay before interacting with the nuclear background, the relatively large $K_L$ lifetime $\tau_{K_L} = 5.1 \times 10^{-8}$ sec may render its impact on the BBN output even more drastic then in the $K^{\pm}$ case. In contrast to $K^{\pm}$, however, $K_L$ are not stopped by electromagnetic interactions so that one should take into account the energy dependence of their cross sections with nucleons. Again, we avoid this complication by assuming the injection of kaons close to the threshold.

For $K_L$-nucleon scattering we exploit charge independence and use isospin relations of the strong interaction processes. Indeed, conservation of strangeness implies that the inelastic scattering of $K_L$ on nucleons essentially resembles the one of $\bar{K}^0$, as $K_L = 2^{-1/2}(K^0 - \bar{K}^0)$ up to small $CP$-violating corrections. Thus, up to corrections due to $K^{\pm}$, $\bar{K}^0$, and $n$, $p$ mass differences and other isospin-violating effects, one finds

$$\sigma(K_L p \to Y\pi) \simeq \tfrac{1}{2}\sigma(\bar{K}^0 p \to Y\pi) \simeq \tfrac{1}{2}\sigma(K^- n \to \tilde{Y}\,\tilde{\pi}), \tag{2.50}$$

$$\sigma(K_L n \to Y'\pi') \simeq \tfrac{1}{2}\sigma(\bar{K}^0 n \to Y'\pi') \simeq \tfrac{1}{2}\sigma(K^- p \to \tilde{Y}'\tilde{\pi}'), \tag{2.51}$$

where $Y$, $Y'(\pi, \pi')$ stands for a hyperon (pion) and $\tilde{Y}$, $\tilde{Y}'(\tilde{\pi}, \tilde{\pi}')$ are the associated states with a flipped third isospin component—the final states of (2.43) and (2.42), respectively. The energy dependence of the cross sections not far from the threshold is inferred from (2.45). Indeed, since (2.50) is a pure $I = 1$ process, $\sigma(K_L p \to Y\pi) = \sigma_1/2$. With the branching fractions (2.44) the inclusive cross sections for $p \to n$ as well as for $n \to p$ conversion are then readily found from (2.50) and (2.51), respectively.

In addition to the reactions listed above, the following processes are possible: $K_L n \to K^- p$, $K_L p \to K^+ n$, and $K_L p \to K_S p$. The cross sections for the former two processes are approximately equal, with $K_L$ scattering being mediated by its $\bar{K}^0$ or $K^0$ component, so that they can be inferred from an expression for $K^- p \to \bar{K}^0 n$ in [56] by detailed balancing. Though the above processes potentially contribute to the loss of $K_L$ and/or generation of $K^{\pm}$, the probability of such processes within a kaon lifetime is very small so that they can be safely neglected. In addition to the processes discussed above, one should again account for the induced charged pion population from to $K_L$ and $K_S$ decays. The respective branching fractions read

$$K_L \to \pi^+ X, \pi^- X\text{: } 46.3\%, \qquad K_S \to \pi^+\pi^-\text{: } 69.2\%, \tag{2.52}$$

where $X$ is the inclusive particle final state without charged pions (not to be confused with $X$ relics). As in the case of charged kaons, the kinetic energy of outgoing pions can be as large as $m_K/2 - m_\pi \simeq 110$ MeV, and already in the regime where $p + \pi^-$ cross sections is enhanced.

Turning to $^4$He-$K_L$ reactions we have just seen that $K_L$ scattering on nucleons can be related to $K^\pm$ reactions using charge independence and isospin symmetry. On these grounds there is no obvious reason to suspect that $K_L$ reactions on helium will be drastically different in magnitude when compared to $K^-$. Thus, by turning off the $K^-$ reactions on helium in the Boltzmann code we can directly assess the difference between the charged and neutral kaon case without attempting to infer the $^4$He-$K_L$ cross sections. Not surprisingly, we then find that whenever the $K_L$ energy in the final state is very small, i.e., on the order of a few MeV, the results for the $K_L$ case are essentially identical to Fig. 7.

To conclude the kaon section, we would like to comment that several avenues for improvement still exist after our analysis. For example, the treatment of pions from kaon decays is done via assigning them a simplistic average energy, while of course a continuous energy spectrum would be required. As seen in the previous section, however, the effect of in-flight pions is not as drastic as naively expected so that the corrections due to continuously distributed $\pi^\pm$ from kaon decays will be only very moderate. Furthermore, the effects of incomplete stopping of $K^-$ and energetic $K_L$ would also need to be included if one intends to explore the BBN sensitivity to a wider range of $m_X$. Here, no further conceptual complications arise and such an analysis can readily be performed by employing a treatment along the lines of the previous section.

### E. Decays to muons and neutrinos

Stopped muons in the final state of the $X$ decay are sourcing energetic muon and electron neutrinos. In order to include these neutrinos in the set of Boltzmann equations we shall use the fact that $\Gamma^\nu_{\rm stop}$ is slower than the Hubble rate. We account for the continuous neutrino injection and energy redshifting by calculating the neutrino phase space distribution function $f(T, E_\nu)$. A previous analysis of BBN modified in the presence of the energetic neutrinos [58] concentrated on the effects of energy deposition and neglected the direct nuclear-chemical impact of neutrinos [59], which turns out to be a more important effect at early times.

The calculation of $f(T, E_\nu)$ depends on the injection rate $\Gamma_{\rm inj}$, and on the primary spectrum of neutrinos at the time of injection,

$$F^0_{e,\mu}(E, E_0) = \begin{cases} \nu_e, \quad \bar\nu_e\text{: } 12E^2(E_0 - E)E_0^{-4} & \text{for } 0 < E < E_0 \\ \nu_\mu, \quad \bar\nu_\mu\text{: } 2E^2(3E_0 - 2E)E_0^{-4} & \text{for } 0 < E < E_0, \\ 0 & \text{for } E > E_0 \end{cases} \tag{2.53}$$

where $E_0 \simeq m_\mu/2$ is the neutrino end-point energy in the muon decay, and $F^0_{e,\mu}$ is normalized to unity, $\int F^0_{e,\mu} dE = 1$. Once injected, neutrinos are subject to flavor oscillations so that the primary energy spectrum will be "distorted." Apart from vacuum oscillations, the neutrino propagation is affected by the coherent neutral and charged current interactions with particles in the primordial plasma. To assess the importance of neutrino-refraction we can compare the vacuum contributions in the neutrino Hamiltonian,

$$\frac{\Delta m^2_{\rm sol}}{4E} \gtrsim 10^{-13}\ \text{eV}, \qquad \frac{|\Delta m^2_{\rm atm}|}{4E} \gtrsim 10^{-11}\ \text{eV}, \tag{2.54}$$

with the matter-induced potential $V_{\rm M}$; $E < E_0$. Here, $\Delta m^2_{\rm sol} \simeq 7.7 \times 10^{-5}\ \text{eV}^2$ and $|\Delta m^2_{\rm atm}| \simeq 2.4 \times 10^{-3}\ \text{eV}^2$ are the respective mass-squared differences responsible for solar and atmospheric neutrino mixing [33]. For $V_{\rm M}$ one can write (see e.g. [60])

$$V_{\rm M} = \pm(8 \times 10^{-19}\ \text{eV}) T_9^3 \times \begin{cases} (-1 + 4Y_{\nu_e} + 3Y_e) & \text{for } \nu_e(\bar\nu_e) \\ (-1 + 2Y_{\nu_e} + Y_e) & \text{for } \nu_{\mu,\tau}(\bar\nu_{\mu,\tau}) \end{cases}, \tag{2.55}$$

where the $Y_i$ denote the particle-antiparticle asymmetries normalized to baryons. The numerical factor in front of (2.55) is $G_F n_b/\sqrt{2}$ with the overall $+(-)$ sign for $\nu(\bar\nu)$. Unlike the case of charged leptons where $Y_e = \mathcal{O}(1)$, the asymmetry in the neutrino sector could be large. In this paper we do not consider such scenarios and limit the asymmetry in the neutrino sector by requiring $|Y_\nu| < 10^4$. The last condition corresponds to $|\xi_\nu| \equiv |\mu_\nu|/T < 5 \times 10^{-5}$ with $\mu_\nu$ being the neutrino chemical potential. Comparing (2.54) with (2.55) then implies that the flavor evolution of injected neutrinos is given by their vacuum oscillations. Note that the restriction on the neutrino chemical potentials also renders neutrino-neutrino self-interactions unimportant which usually have the effect

of locking the neutrino modes to each other, leading to a coherent oscillatory behavior [61].

A major simplification in the calculation of $f(T, E_\nu)$ occurs due to the large rates for vacuum oscillations,

$$\Gamma_{i,\mathrm{osc}} = 1.2 \times 10^8 \left(\frac{1\ \mathrm{MeV}}{E}\right)\left(\frac{|\Delta m_i^2|}{1\ \mathrm{eV}^2}\right) \gtrsim \begin{cases} 175\ \mathrm{sec}^{-1} & i = \mathrm{sol} \\ 5.5 \times 10^3\ \mathrm{sec}^{-1} & i = \mathrm{atm} \end{cases}, \quad (2.56)$$

compared to the Hubble rate and the neutrino injection rate, $\Gamma_{i,\mathrm{osc}} \gg H, \Gamma_X$. This allows us to replace the primary injection spectrum $F_e^0$ in (2.53) by an effective one,

$$F_e = \langle P_{ee}\rangle F_e^0 + \langle P_{\mu e}\rangle F_\mu^0, \quad (2.57)$$

where the $\langle P_{ee}\rangle$ and $\langle P_{\mu e}\rangle$ are the $\nu_e(\bar\nu_e)$-survival and $\nu_\mu(\bar\nu_\mu) \to \nu_e(\bar\nu_e)$-appearance probabilities, averaged over oscillations,

$$\langle P_{ee}\rangle = 1 - \tfrac{1}{2}\sin^2 2\theta_{12} \simeq 0.57, \quad (2.58)$$

$$\langle P_{\mu e}\rangle = \langle P_{e\mu}\rangle = \tfrac{1}{2}\sin^2 2\theta_{12}\cos^2\theta_{23} \simeq 0.23. \quad (2.59)$$

The vacuum mixing angles are given by $\sin^2\theta_{12} = 0.312$ and $\sin^2\theta_{23} = 0.466$ [33] and we have assumed $\theta_{13} = 0$. Note that (2.57) already accounts for the appropriate reduction of the electron neutrino flux due to $\nu_e(\bar\nu_e) \to \nu_\mu(\bar\nu_\mu)$ and $\nu_e(\bar\nu_e) \to \nu_\tau(\bar\nu_\tau)$ disappearances.[1]

Defining $f(T, E_\nu)$ in such a way that $\int f(T, E_\nu) dE_\nu$ is equal to the total number of energetic neutrinos per baryon, we arrive at the neutrino distribution function,

$$f_e(T, E_\nu) = \int_T^\infty \frac{dT_1 \Gamma_{\mathrm{inj}} Y_X(T_1)}{H(T_1) T_1} F_e\left(E_\nu, \frac{E_0 T}{T_1}\right), \quad (2.60)$$

where $\Gamma_{\mathrm{inj}} = \Gamma_X$ since we assume that the neutrino-sourcing muons result from the decays of the $X$ relics.

Electron antineutrinos will have the largest effect on the BBN network. Integrated with the weak cross section over energy, the distribution function gives the energetic neutrino-induced rate of $p \to n$ conversion:

$$\bar\nu_e + p \to n + e^+ : \Gamma_{pn}^\nu = n_b(T) \int_0^{E_0} \sigma_{pn}^{\bar\nu}(E_\nu) f_e(T, E_\nu) dE_\nu, \quad (2.61)$$

where $n_b(T)$ is the number density of baryons at temperature $T$. The cross section for quasielastic neutrino nucleon scattering reads (see e.g. [62])

$$\sigma_{pn}^{\bar\nu}(E_\nu) = 0.0952 \times 10^{-42} \left(\frac{p_e E_e}{1\ \mathrm{MeV}^2}\right) S(E_\nu)\ \mathrm{cm}^2, \quad Q \simeq -1.8\ \mathrm{MeV}, \quad (2.62)$$

where $E_\nu$ and $E_e = E_\nu - \Delta m_{np}$ are the energies of $\bar\nu_e$ and $e^+$ in the rest frame of the proton, respectively; $\Delta m_{np} \simeq 1.293\ \mathrm{MeV}$ is the neutron-proton mass difference and $p_e$ is the positron momentum. We introduce a correction factor $S(E_\nu) = (1 - 0.0063 E_\nu/\mathrm{MeV})$ which improves the agreement between the simple formula (2.62) and a precise evaluation of $\sigma_{pn}^{\bar\nu}$ in [63] to better than 1% in the $E_\nu$ regime of interest.

In our code we also account for exoergic $n \to p$ conversions via $\nu_e + n \to p + e^-$. This process, however, is only important for $\tau_X \lesssim 180$ sec, i.e., prior to $n$ consumption by $^4$He. The associated cross section $\sigma_{np}^\nu(E_\nu)$ is obtained from (2.62) with $E_e = E_\nu + \Delta m_{np}$ and $S(E_\nu) = 1$. As in (2.61) we average $\sigma_{np}^\nu(E_\nu)$ over $f_e$ in order to obtain the rate $\Gamma_{np}^\nu$ for $n \to p$ conversion.

Muon neutrions $\nu_\mu$ and $\bar\nu_\mu$ which are sourced from muon decays (at rest) are not capable of interconverting protons and neutrons as their maximum injection energy $m_\mu/2$ lies below the reaction threshold $\mathcal{O}(100\ \mathrm{MeV})$. However, $\nu_\mu(\bar\nu_\mu)$ along with $\nu_{e,\tau}(\bar\nu_{e,\tau})$ are in principle capable of dissociating $^4$He via their neutral current interactions. Among the possible final states, only the ones with mass-3 elements have an appreciable cross section in the low-energy regime $E_\nu < m_\mu/2$ [64]. We include the following neutral current (NC) and charged current (CC) reactions into our Boltzmann network:

$$\mathrm{NC}: \begin{cases} {}^4\mathrm{He} + \overset{(-)}{\nu}_{e,\mu,\tau} \to \overset{(-)}{\nu}_{e,\mu,\tau} + p + \mathrm{T} \\ {}^4\mathrm{He} + \overset{(-)}{\nu}_{e,\mu,\tau} \to \overset{(-)}{\nu}_{e,\mu,\tau} + n + {}^3\mathrm{He} \end{cases}, \quad \mathrm{CC}: \begin{cases} {}^4\mathrm{He} + \nu_e \to e^- + p + {}^3\mathrm{He} \\ {}^4\mathrm{He} + \bar\nu_e \to e^+ + n + \mathrm{T} \end{cases}. \quad (2.63)$$

For the NC reactions of muon and tau neutrinos we infer the reaction rates averaged over $f_{\mu,\tau}$ by following the same logic from (2.57) through (2.60). For the cross sections we use fitting formulas interpolating the tables provided in [64].

Given that the efficiency for neutron-to-proton conversion per each injected neutrino is so low [cf. (2.24)], a high initial $X$-abundance (in comparison to baryons) is needed in order to achieve an appreciable reduction of $^7\mathrm{Li} + {}^7\mathrm{Be}$. In our code we take the extra contribution of $\rho_X$ to the total energy density into account. By comparing $\rho_X$ (prior to decay) with the radiation energy density $\rho_{\mathrm{rad}}$,

$$\frac{\rho_X}{\rho_{\mathrm{rad}}} \simeq \frac{10^{-6} Y_X}{T_9}\left(\frac{m_X}{1\ \mathrm{GeV}}\right), \quad (2.64)$$

we see that a GeV-scale relic $X$ starts contributing to the Hubble rate appreciably during BBN for $Y_X \gtrsim 10^5$.

In Fig. 8 we show the results of our computation for $X \to \mu^+\mu^-$ in the usual $(\tau_X, \xi_\mu^{(X)} Y_X)$ plane for $\xi_\mu^{(X)} = 1$. For simplicity, again, we assume the muon injection close to the kinematic threshold, $m_X = 2m_\mu$, although

[1] In a similar fashion, $F_\mu = \langle P_{\mu\mu}\rangle F_\mu^0 + \langle P_{e\mu}\rangle F_e^0$ and $F_\tau = \langle P_{e\tau}\rangle F_e^0 + \langle P_{\mu\tau}\rangle F_\mu^0$ with $\int dE(F_e + F_\mu + F_\tau) = 2$.

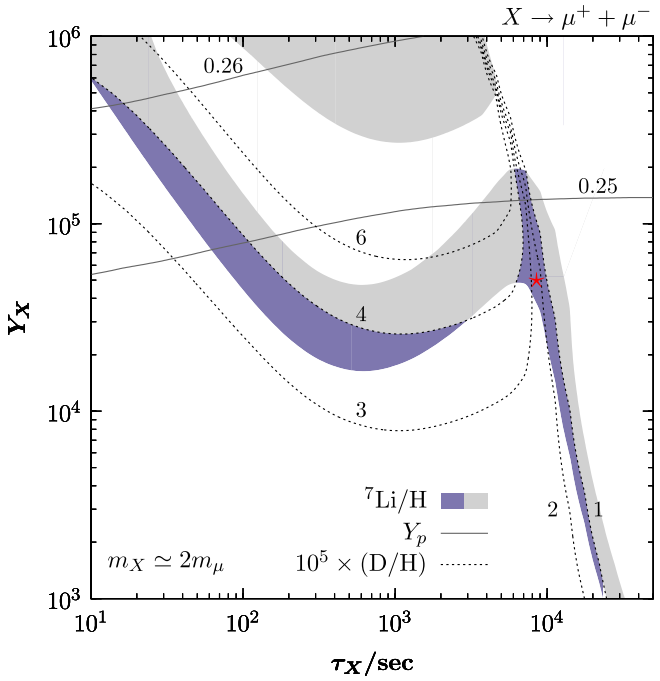


FIG. 8 (color online). Same as in Fig. 5, but for $X$ decaying into $\mu^+\mu^-$ pairs which eventually decay into neutrinos (and $e^\pm$). Note the smaller values $\tau_X$ in comparison to the previous figures. Energetic neutrinos are accumulating over time so that $X$ decays as early in time as $t = 10$ sec can affect the BBN network. Noteworthy is also the increased $^4$He abundance for large values of $Y_X$ over the whole $\tau_X$ range since the $X$-matter density is contributing to $H$. In this figure, $m_X \simeq 2m_\mu$. A novel feature is also the appearance of a second observationally favored region for $\tau_X \simeq 10^4$ sec. No additional $^6$Li in excess of SBBN values is produced and electromagnetic energy injection depletes previously formed D/H. For the parameters marked by the star the temporal evolution of the light elements is shown in Fig. 9.

this assumption is less crucial compared to the hadronic case. Note that this time we have extended the $\tau_X$ range to lifetime values as small as 10 sec. This is because the usual temporal correlation between $X$ decay and its effect on the BBN yields breaks down. For example, neutrinos injected at $t = 10$ sec may still induce $p \longrightarrow n$ conversion at $t = 100$ sec. As expected, the results show a similar pattern as in the pion and kaon cases with $Y_X$ scaled to larger values. In the neutrino case, however, one finds an increased $^4$He abundance for $Y_X \gtrsim 10^5$ over the whole $\tau_X$ range. This is because the $X$ energy density is contributing to the Hubble rate, leading to an earlier $n/p$ freeze-out and thereby to a higher $^4$He abundance. Though this makes results sensitive to $m_X$, it is nevertheless only a mild dependence for $m_X \lesssim 1$ GeV in the interesting region $Y_X \sim 10^4$, in which lithium is reconciled with observations. As it further turns out, the neutrino reactions dissociating $^4$He are giving at most a marginal correction to the BBN yields even for $X$ abundances as high as $Y_X = 10^6$. The reasons are that the processes of (2.63) possess threshold energies $E_{\rm th} \sim 20$ MeV and because the associated cross sections are significantly smaller in comparison to (2.62). This has another interesting consequence: in contrast to the pion and kaon scenarios essentially no $^6$Li is produced for $\tau_X \gtrsim 10^4$ sec, allowing for a second region of cosmologically favored $^7$Li abundances in which high D/H is also photodissociated. As discussed earlier, this region is necessarily fine-tuned in $\tau_X$ because of the exponential sensitivity in injected electromagnetic energy. Indeed, for even larger lifetimes $\tau_X \gtrsim 10^6$ sec one would observe what could be called the "photodissociation catastrophe" with $^4$He along with all other elements being dissociated (for large enough $Y_X$). Nevertheless, we find this scenario rather distinct if not remarkable. The injection of muons with relic $X$ decays with lifetimes of $10^4$ sec is capable of reducing the $^7$Li abundance while keeping other abundances close to the their SBBN-predicted values. This occurs because of the nonmonotonic evolution of D/H: the increase due to neutrino-induced neutron enrichment is followed by the decrease due to energy injection.

The temporal evolution of elemental abundances for a single point in the parameter space marked by the star in Fig. 8 is illustrated in Fig. 9. The most prominent feature is the "bump" in the neutron abundance at $T_9 \sim 0.06$

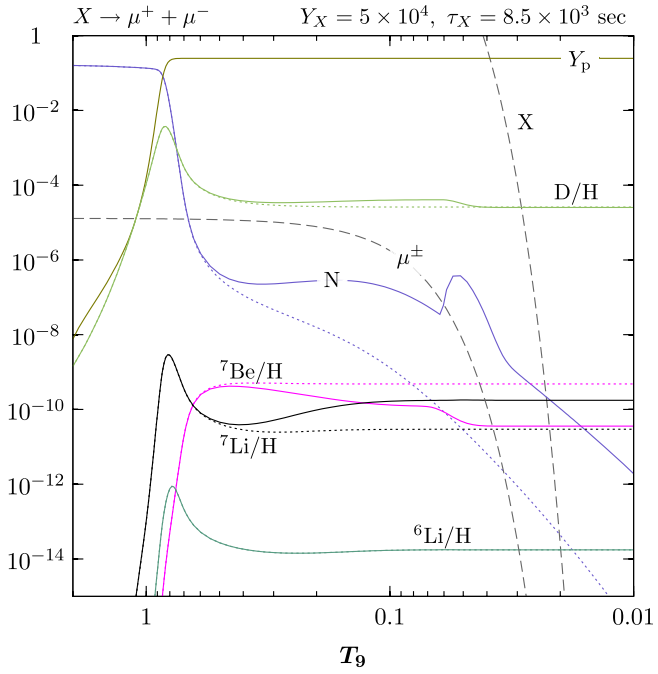


FIG. 9 (color online). Temperature evolution of light nuclei, metastable parent $X$ particles and daughter $\mu^\pm$ for $Y_X = 5 \times 10^4$ prior to decay and $\tau_X = 8.5 \times 10^3$ sec. Starting off with the previously observed effects which are induced by an elevated neutron abundance (suppressed $^7$Be/H, elevated D/H), electromagnetic energy injection eventually dissolves deuterium and beryllium for $T_9 \lesssim 0.06$. This not only reinstates the SBBN D/H prediction (corresponding dotted line) but also implies that lithium is mainly produced in the form of $^7$Li.

marking the point in time in which deuterium is subjected to photo destruction. The associated decrease in D/H from its elevated values down to its original SBBN prediction (dotted lines) are clearly seen in this figure. Also $^7$Be is dissociated around the same time so that the overall lithium abundance comes essentially in the form of $^7$Li.

## III. METASTABLE GEV-SCALE STATES AND THE LITHIUM ABUNDANCE

In this section we consider some specific models of GeV-scale relics and their impact on the BBN predictions. All models can be subdivided into broad categories of WIMPs and super-WIMPs, where "super" refers to the superweak interaction strength with SM states. WIMPs are thermally excited above their mass scale, then depleting their number density via annihilation at $T < m_{\rm WIMP}$, and—in our case—decaying after the start of BBN. Superweakly interacting particles typically have very small production rates throughout the whole history of the Universe. This justifies the assumption of super-WIMPs being initially absent as the Universe enters its thermal radiation-dominated stage, e.g., after inflation and reheating, so that only some small super-WIMP abundance develops due to the thermal leakage from the SM states. Let us stress again that the notion of a (super)WIMP here is not to be confused with a dark matter state (which has to be stable on cosmological timescales.) Of course, some of the metastable particles presented in this section are motivated by their potential as mediators of the interactions between dark matter particles and the SM sector [27,65].

The simplest WIMP model without any need of UV completion [66,67] uses the so-called Higgs portal. In this model, a singlet scalar field $S$ interacts with the rest of the SM via its coupling to the Higgs doublet $H$,

$$\mathcal{L}_{\rm H-portal} = \tfrac{1}{2}(\partial_\mu S)^2 - V(S) - (\lambda S S + A S)(H^\dagger H). \quad (3.1)$$

Here we assume an approximate $Z_2$ symmetry, $S \to -S$, broken only by the last trilinear term $AS(H^\dagger H)$, and we further take $A$ to be very small; $V(S)$ is the scalar potential in the secluded sector. If the $\lambda$ coupling is above $O(10^{-10})$, the $S$ particles are guaranteed to be in thermal equilibrium with the SM states as soon as the plasma temperature is around the electroweak scale. Smaller values of $\lambda$ make $S$ to a super-WIMP [68]. The physical mass of $S$ particles comes from the potential term $m_0^2 S^2/2$ and the electroweak vacuum expectation value $v \simeq 246$ GeV, $m_S^2 = m_0^2 + \lambda v^2$. Having

$$A,\ \lambda, \quad \text{and } m_S^2 \ (\text{S} - \text{portal}) \quad (3.2)$$

at our disposal, we can always choose the region of parameter space where the lithium abundance is reduced along the lines described in the previous section. Of course, in this model the GeV scale is not special, and metastable $S$ particles at the electroweak scale can also be used for the same purposes, exploiting nucleons in the decay products of $S$.

Going away from the simplest possibility, we introduce a U(1)$_S$ vector portal model [69],

$$\mathcal{L}_{\rm V-portal} = -\frac{1}{4}V_{\mu\nu}^2 - \frac{\kappa}{2}F^Y_{\mu\nu}V^{\mu\nu} + |D_\mu\phi|^2 - V(\phi), \quad (3.3)$$

where the connection between the U(1)$_S$ field strength $V_{\mu\nu}$ and the hypercharge field strength $F^Y_{\mu\nu}$ is mediated via the kinetic mixing parameter $\kappa$. The U(1)$_S$ covariant derivative is given by $D_\mu = \partial_\mu + ie' V_\mu$, with $V_\mu$ being the new vector-state associated with $V_{\mu\nu}$ and $e'$ the gauge coupling strength in the secluded sector.

Since we are going to consider GeV-scale phenomenology, one can substitute the hypercharge with the photon field strength, $F^Y_{\mu\nu} \to F_{\mu\nu}$ and absorb the cosine of the Weinberg angle into the new definition of $\kappa$. After the spontaneous breaking of the U(1)$_S$ gauge group by a Higgs$'$ field $\phi$, the low-energy Lagrangian can be written as

$$\mathcal{L} = -\tfrac{1}{4}V_{\mu\nu}^2 + \tfrac{1}{2}m_V^2 V_\mu^2 + \tfrac{1}{2}(\partial_\mu h')^2 - \tfrac{1}{2}m_{h'}^2 h'^2 + \mathcal{L}_{\rm int}, \quad (3.4)$$

where $m_V = e' v'$ becomes the mass of $V_\mu$ and $m_{h'}$ is the mass of the physical Higgs$'$ field $h'$, $\langle\phi\rangle = v'/\sqrt{2}$. Assuming a standard Higgs potential in the U(1)$_S$ sector, the interaction terms are given by

$$\mathcal{L}_{\rm int} = -\frac{\kappa}{2}V_{\mu\nu}F^{\mu\nu} + \frac{m_V^2}{v'}h' V_\mu^2 + \frac{m_V^2}{v'^2}h'^2 V_\mu^2 - \frac{m_{h'}^2}{2v'}h'^3 - \frac{m_{h'}^2}{8v'^2}h'^4. \quad (3.5)$$

Thus, like in the previous example, the model is characterized by only a handful of free parameters:

$$\alpha',\ \kappa,\ m_{h'}, \quad \text{and } m_V \ (\text{V} - \text{portal}), \quad (3.6)$$

where, as usual, $\alpha' = e'^2/4\pi$. The strength of the mixing angle $\kappa$ is undoubtedly a very important parameter, as it allows us to make the link between the SM and U(1)$_S$ sector arbitrarily weak. Indeed, for $\kappa < 10^{-12}$ any production rate of $h'$ and $V$ particles is smaller than the Hubble rate, and the model becomes a good candidate for the superweak regime. It is also important to notice that long lifetimes of particles from the U(1)$_S$ sector can be achieved *without* requiring exceedingly small $\kappa$. This happens rather naturally in the regime $m_{h'} < m_V$, where the decay amplitude of the Higgs from the secluded sector is suppressed by $\kappa^2$ [32,70]. As mentioned in the Introduction, the (sub)-GeV mass scales for U(1)$_S$ states are motivated by the possible enhancement of the annihilation of weak-scale WIMPs into leptons [23,24].

### A. WIMP regime

Here we would like to determine the values of parameters for both models, (3.2) and (3.6), that lead to the desirable depletion of the $^7$Li abundance. Since in the WIMP regime the coupling constants are not necessarily small, the results of this subsection might be relevant for the direct searches of new physics at GeV energy scales.

For the Higgs portal model in the WIMP regime there are several generic choices of parameters that lead to the desirable range of the lifetime–mass-abundance "islands" that suppress the overall lithium abundance. These regions can be readily found using the results for the lifetime [71] and freeze-out abundance of $S$ particles [67,72,73]. For example, the following choice of parameters,

$$Y_S \simeq 3\times 10^4, \qquad \tau_X \sim 500 \text{ sec}, \qquad m_S = 250 \text{ MeV}$$
$$\Rightarrow \lambda^2 \simeq 2\times 10^{-2}, \qquad A = 4\times 10^{-8} \text{ GeV}, \tag{3.7}$$

leads to the depletion of lithium via the decays of $S$ particles to muon pairs, generating electron antineutrinos. Higher masses of $S$ particles, $m_S > 2m_\pi$ that generate hadrons in the decay product would typically require $\lambda \sim O(1)$ in order to have $Y_S \lesssim 10^2$. The estimate (3.7) is performed for a Higgs mass value of 100 GeV but can be easily rescaled for heavier values. Notice that the $A$ parameter does not enter in the abundance calculation, and can always be adjusted to obtain a desirable lifetime.

Interestingly enough, the mass range of $m_S \lesssim 2$ GeV is being probed through the search of missing energy decays of $B$ mesons, $B \to K^{(*)}SS$, [72–74] as the eventual decays of $S$ particles occur far away from the $B$-decay vertex. When the phase space suppression can be neglected, the prediction for the missing energy branching ratio at $m_h = 100$ GeV is $\text{Br}_{B\to K\not{E}} \sim 4\times 10^{-6} + 3\times 10^{-4}\lambda^2$ [72], where the first term stands for the SM contribution via $B \to K\nu\bar{\nu}$. The current upper bound on the branching ratio stands at $1.5\times 10^{-5}$, excluding models with $\lambda \sim O(1)$. The choice of parameters (3.7) is still (barely) allowed, both by the $B$ and $K$ decays with missing energy. We conclude that only this low $m_S$ option (or alternatively $m_S \gtrsim 2$ GeV) is capable of solving the lithium problem without enhancing the missing energy branching ratios of $B$ mesons beyond what is observed. Perhaps the most interesting consequence of large values for $\lambda$ required by the solution to the lithium problem are the implications for Higgs physics. For Higgs masses of 150 GeV and lighter the missing energy decays $h \to SS$ will dominate over the standard model width and lead to a significant enhancement of the missing energy channel and suppression of visible decay modes [67]. In short, the viability of the proposed scenario will be tested at the LHC, (super)$B$ factories and new kaon facilities.

Metastable GeV-scale particles from a U(1)$_S$ sector is another interesting possibility. In the WIMP regime we are drawn to consider $h'$ since the vectors $V$ decay well before BBN through their now appreciable kinetic mixing $\kappa \gg 10^{-10}$ [see Eq. (3.18) below],

$$\tau_V \leq 0.05 \text{ sec} \times \left(\frac{10^{-10}}{\kappa}\right)^2 \left(\frac{500 \text{ MeV}}{m_V}\right) \quad \text{for } m_V \gtrsim m_e. \tag{3.8}$$

Indeed, the longevity of $h'$ particles can be achieved rather naturally in the regime $m_{h'} < m_V$. The lifetime of the $h'$ particles due to the four-body decays and one-loop induced amplitudes was calculated in Ref. [75]. For example, the decay width to muons in the regime $2m_\mu < m_{h'} \ll m_V$ is dominated by loop effects and is given by

$$\tau_{h'} \sim (10^3 \div 10^4) \text{ sec} \times \left(\frac{\alpha}{\alpha'}\right)\left(\frac{3.4\times 10^{-5}}{\kappa}\right)^4 \left(\frac{250 \text{ MeV}}{m_{h'}}\right) \times \left(\frac{m_V}{500 \text{ MeV}}\right)^2. \tag{3.9}$$

This formula remains approximately valid in the regime $m_{h'} \sim m_V$, and breaks down at $m_V - m_{h'} \ll m_{h'}$. With $m_V \sim 500$ MeV and $\alpha' \sim \alpha$ it is easy to see that for $m_{h'} = 250$ MeV and $\kappa \simeq (3 \div 10)\times 10^{-5}$ the decay rate of $h'$ is in the right ballpark, while for the same value of couplings and masses the decay of vectors happens very fast, $\tau_V < 10^{-16}$ sec.

Since we take the $h'$ particle to be the lightest in the U(1)$_S$ sector and long-lived, what physical mechanisms could possibly deplete its abundance to an acceptable level? It turns out that possible *endothermic* excitations into the $V$ state, $h' \to V$ followed by $V$ decays, although exponentially sensitive to the mass parameters in the U(1)$_S$ sector, are in principle sufficient for the $h'$ depletion.[2] In particular, the following processes are capable of suppressing the $h'$ abundance:

$$h' + h' \to V + V\text{: } \Gamma_1 \propto (\alpha')^2\kappa^0 \exp(-m_{h'}/T - 2\Delta m/T), \tag{3.10}$$

$$h' + V \to l^+l^-\text{: } \Gamma_2 \propto \alpha'\alpha\kappa^2 \exp(-m_{h'}/T - \Delta m/T), \tag{3.11}$$

$$h' + l^\pm \to V + l^\pm\text{: } \Gamma_3 \propto \alpha'\alpha\kappa^2 \exp(-\Delta m/T), \tag{3.12}$$

where $\Delta m = m_V - m_{h'}$, and $l^\pm$ are the charged particles of the SM. The last process in (3.12) is especially important because it comes with the least amount of exponential suppression. We now estimate the freeze-out abundance of $h'$ due to this process.

In the nonrelativistic regime, the equilbrium number density $n_{h'}^{\text{eq}}$ of $h'$ follows the well-known curve, and the freeze-out abundance can be estimated by equating the depletion rate $\Gamma_3$ with the Hubble rate, $H(T_f) = \Gamma_3(T_f)$,

[2] M. P. would like to thank Neal Weiner for a very useful discussion of that point.

$$Y_{h'} \simeq n^{eq}(T_f)/n_b(T_f), \tag{3.13}$$

$$n^{\rm eq}_{h'}(T) = \left(\frac{m_{h'}T}{2\pi}\right)^{3/2} \exp(-m_{h'}/T). \tag{3.14}$$

We would like to determine the dependence of the freeze-out temperature $T_f$ on $\Delta m$, and specialize it to two cases considered in the previous section: decays to muons and decays to pions/kaons. Considering the exponential dependence on the mass splitting $\Delta m$ we are making a series of simplifying approximations: $m_e \ll T_f \ll \Delta m \ll m_V, m_{h'}$. In that case the cross section for the $h' + e^{\pm} \to V + e^{\pm}$ process is given by

$$\sigma = \frac{16\pi\kappa^2\alpha\alpha'}{m_V^4}\,\frac{\Delta m(E_e - \Delta m)^2}{E_e}$$
$$\Rightarrow \Gamma_3(T) \simeq \frac{64\kappa^2\alpha\alpha' T^3(\Delta m)^2}{\pi m_V^4}\exp(-\Delta m/T), \tag{3.15}$$

where $E_e$ is the electron energy. For $T_f$ larger than 100 MeV, other charged SM states would have to be included in the coannihilation process (3.12). However, since we are in need of a suppression of the $h'$ abundance by a large factor, the freeze out of a GeV scale $m'_h$ has to happen below 100 MeV, so that only $e^{\pm}$ will contribute to depletion process.

Introducing two dimensionless variables $x_f = m_{h'}/T_f$ and $\delta = \Delta m/m_{h'} = m_V/m_{h'} - 1$, we arrive at the following analytic estimate of the freeze-out temperature and the resulting abundance as a function of mass splitting in the $U(1)_S$ sector:

$$x_f \simeq \frac{1}{\delta}\left\{13 + \ln\left[\frac{\alpha'}{\alpha}\,\frac{\delta^2}{(1+\delta)^4}\,\frac{15}{x_f}\left(\frac{\kappa}{3\times 10^{-5}}\right)^2\frac{250\ \text{MeV}}{m_{h'}}\right]\right\}, \tag{3.16}$$

$$Y_{h'} \simeq 4.2\times 10^8 \times x_f^{3/2}\exp(-x_f). \tag{3.17}$$

It is easy to see that for mass splittings $\delta \simeq 0.3 \div 0.5$ the abundance varies in the interval $10^{-1} \div 10^2$, which will be suitable for the solution of the lithium problem using the decays of $h'$ to pions and kaons. Mass splittings of order $\delta \simeq 0.8 \div 1.4$ correspond to abundances on the order $10^4 \div 10^6$, which are suitable for suppressing lithium via the decays of $h'$ to muons. We remark in passing that (3.17) represents the fraction of $h'$ relative baryons after $e^{\pm}$ annihilation but prior to their decay.

Since the realization that a new attractive $U(1)_S$ gauge force can be used for the explanation of the PAMELA anomaly [23,24], a lot of dedicated work has been done in order to understand the prospects of searching/detecting particles from a putative $U(1)_S$ sector. The most promising avenues for the discovery of new GeV-scale particles are high-luminosity medium-to-low-energy experiments [75–77], although some prospects of discovering such particles in the fragmentation of heavy exotic particles produced in the high-energy collisions have also been investigated [78]. The mixing angles deduced in this section, $\kappa \sim 3\times 10^{-5}$, and vector masses in the range of 400 MeV and larger, represent one of the most challenging corners in the $m_V$-$\kappa$ parameter space. These angles are small enough so that the search of $V$ in this range at even the highest luminosity $e^+e^-$ machines is not possible. Therefore, the search for $V$ in this regime with fixed target experiments is perhaps the only realistic option. Vector particles are relatively short lived, $c\tau \leq 1$ cm, so that in the setup with a detector at some macroscopic distance behind the target all the decays will happen before reaching the detector. With proton beams, where the detector is typically tens or hundreds of meters behind the target, such a search might prove to be very challenging. Therefore, the best discovery potential for $V$ in this parameter range would probably be a high-intensity electron beam on a thin target [79]. Lastly, the lifetimes of mediators in excess of milliseconds lead to interesting effects in the annihilation of dark matter, when the decays of mediators occur away from the point where the annihilation occurs [80–82]. This leads to novel signatures in the indirect detection of dark matter in models with light mediators. Finally, for overdensity constraints on some variants of these models see, e.g., [83].

### B. GeV-scale super-WIMPs

In the previous examples we considered metastable particles that initially had thermal abundances. This is not the only possibility, and in the following we will look at the abundances of vectors $V$ and scalars $S$ in the super-WIMP regime. Our assumption is that the link between the SM and the secluded sectors is extremely weak, and given by a single parameter, $\kappa$ for (3.3), and $A$ for (3.1). The states $X = S$ or $V$ are then produced with sub-Hubble rates from the thermal scattering of SM particles. In this case, both the production and the decay rates are proportional to the square of the small parameters $\kappa$ or $A$. Consequently, the product of abundance and lifetime, $Y_X\tau_X$ is independent of $A$ or $\kappa$ and is only a function of the mass $m_X$ and the SM couplings/masses. This scaling holds for both cases despite the fact that the physical production mechanisms of $S$ and $V$ are vastly different. An extra vector particle that appears just as another massive photon is mostly produced at temperatures comparable to its mass $T \gtrsim m_V$ whereas a scalar particle with mixing to the Higgs boson is most efficiently produced at $T \sim m_W$, where the $T/m_h$ dependence of the production rate relative to the Hubble rate is maximized.

We begin by analyzing the $U(1)_S$ model (3.3) in the super-WIMP regime. The decay widths of the vector particles to leptons and hadrons are given by [75]

$$\Gamma_{V\to\bar{l}l} = \frac{1}{3}\alpha\kappa^2 m_V \sqrt{1-\frac{4m_l^2}{m_V^2}}\left(1+\frac{2m_l^2}{m_V^2}\right), \tag{3.18}$$

$$\Gamma_{V\to\text{hadrons}} = \frac{1}{3}\alpha\kappa^2 m_V \sqrt{1-\frac{4m_\mu^2}{m_V^2}}\left(1+\frac{2m_\mu^2}{m_V^2}\right)R(s=m_V^2), \tag{3.19}$$

where $R$ is the experimentally measured ratio of the inclusive hadroproduction in $e^+e^-$ collisions to the direct muon production, $R = \sigma_{e^+e^-\to\text{hadrons}}/\sigma_{e^+e^-\to\mu^+\mu^-}$. It follows immediately [see also Eq. (3.8)] that a desirable lifetime range $\tau_V \gtrsim \mathcal{O}(100\ \text{sec})$ requires $\kappa$ in the ballpark of $10^{-12}$.

The production of GeV-scale $V$ bosons in the early Universe cannot be calculated "exactly" because of the unsurmountable difficulty in treating hadrons in the intermediate regime $T \sim \Lambda_{\text{QCD}}$. In particular, all production modes involving free quark and gluons, $q\bar{q} \to V$, $q + g \to q + V$ etc. are not calculable because of the strong QCD coupling. Cases that can be reliably calculated are $m_V \ll 100$ MeV and $m_V \gg 1$ GeV, which are, unfortunately, exactly opposite to the regime we are interested in. Nevertheless, we can obtain an order-of-magnitude estimate that captures the main behavior of the production mechanism as a function of $m_V$. The main feature of the production mechanism is that it receives an exponential cutoff $\exp(-m_V/T)$ in regime $T < m_V$, and this property is not modified by strong dynamics. Therefore, the production effectively stops at $T \sim m_V$ with the residual abundance of $V$ particles parametrically dependent on the ratio of the production rate over the Hubble rate,

$$Y_V = \left.\frac{s}{n_b}\frac{n_V}{s}\right|_f \simeq (1.2 \div 4.9)\times\frac{s}{n_b}\frac{1}{h_{\text{eff}}(m_V)}\frac{\Gamma_{V\to e^+e^-}}{H(m_V)} \sim 0.3\times\left(\frac{10^3\ \text{sec}}{\tau_V}\right)\left(\frac{\text{GeV}}{m_V}\right)^2\left(\frac{40}{g_{\text{eff}}}\right)^{3/2}. \tag{3.20}$$

The estimated range follows from a computation of the collision integral for the inverse decays of Fermi-Dirac distributed pairs $e^\pm$ (lower value) and massless $e^\pm$, $\mu^\pm$, $u\bar{u}$, $d\bar{d}$, $s\bar{s}$ (upper value); for a related calculation see also [84]. The upper value is saturated for freeze-out temperatures above the QCD hadronization scale, $\Lambda_{\text{QCD}} < T_f \lesssim \mathcal{O}(1\ \text{GeV})$, where the perturbative treatment of the light quarks becomes accessible. On the other hand, lower mass vectors whose production ceases later are guaranteed to receive a contribution to their abundance from electron-positron pairs. This limits $Y_V$ from below. In the last relation we have normalized the effective number of entropy degrees of freedom $h_{\text{eff}} \simeq g_{\text{eff}}$ on a typical value during the QCD hadronization epoch and further made the assumption that $\tau_V$ is dominated by the channels which are also responsible for the inverse decay.

The results suggest that a sub-GeV state with a lifetime of the order of a thousand seconds is abundant enough to produce $\mathcal{O}(1)$ pions/kaons per baryon, and thus capable of reducing the lithium abundance by a factor of a few. In the most optimal range with $m_V \sim m_\rho$, the pion branching dominates over lepton branching, while the energy of injected pions is close to the delta-resonance. This enhances the efficiency of $p \to n$ conversion, Fig. 6, so that $Y_V \sim 2$ is required. Since $Y_V$ is not calculable exactly, it is unfortunately not possible to give a final judgement whether the required abundance can be achieved or falls marginally short. We also notice that $m_V$ below the di-pion threshold, $2m_\mu < m_V < 2m_\pi$ can only be created in abundances less than $\mathcal{O}(10^2)$ which renders this parameter range incapable of reducing lithium via $V$-decays into muons. On the other hand, a heavier mass range for a super-WIMP $V$ is also interesting. For example, $V$-bosons in the mass range of 10 GeV or more are less abundant than protons, but will contain nucleons among their decay products. In this case one can easily suppress the lithium abundance via direct injection of extra nucleons along the lines of Refs. [7,8].

The model with the singlet $S$ mixed to the Higgs boson via the $ASH^\dagger H$ coupling can be treated very similarly. Interestingly, it turns out that in this model the abundance of $S$ particles can be calculated without significant QCD uncertainties because it dominantly occurs at electroweak-scale temperatures, whereas the lifetime of the $S$ boson with a mass in the GeV range is notoriously difficult to handle.

In principle many SM scattering processes may contribute to the emission of the $S$ boson. These include $f_1\bar{f}_2 \to VS$, $f_1V \to f_2S$, $hh \to SV$, $VV \to SV$, $tg \to tS$, $t\bar{t} \to gS$ etc., where $f_1$, $f_2$ stand for the SM fermions, $V = W, Z$ for massive gauge bosons, and $g$, $t$ are gluons and top quark. An exact treatment of the production mechanisms in this model falls outside the scope of this paper. However, despite this rather large number of production channels, the asymptotic behavior of the production mechanisms are quite obvious. In the regime $T \gg v$ the production rate has to scale as $\Gamma \propto A^2/T$, and in the low-energy regime it is $\propto A^2T^3m_h^{-4}$. This implies that $\Gamma$ is naturally peaked at temperatures around the electroweak scale.

In order to avoid straightforward but tedious calculations of the $S$ abundance in the most minimal model (3.1), we go to the two-Higgs doublet model analogue of (3.1), and couple the $S$ scalar to a "mixed" Higgs portal:

$$ASH^\dagger H \to \tfrac{1}{2}AS(H_1H_2 + \text{H.c.}). \tag{3.21}$$

Assuming a mild hierarchy of scales in the Higgs sector together with a ratio of the Higgs vacuum expectation values $\tan\beta = v_2/v_1 \gg 1$, $H_2$ represents the SM Higgs doublet while $H_1$ contains heavier physical scalars $H$, $A$, $H^\pm$ with common mass scale $m_H$. The production of scalars $S$ is peaked around $m_H$. In what follows we

calculate the abundance of $S$ resulting from $H_1 \to H_2 S$ decays using $m_H \gg m_h, m_{W(Z)}$. In an exact analogy to (2.10) the decay rate can be written as $\Gamma_H \langle m_H/E \rangle$, where

$$\Gamma_H = \frac{A^2}{16\pi m_H} \tag{3.22}$$

is the decay rate of $H_1$ particles at rest. Accounting for that $H_1$ carries 4 degrees of freedom we arrive at the following integral formula for the freeze-out (or rather "freeze-in") abundance of $S$ bosons realtive to baryons:

$$Y_S = \frac{s}{n_b} \int \frac{m_H dT}{H(T) T s(T)} \int \frac{4 d^3 p}{E (2\pi)^3} \frac{\Gamma_H}{\exp(E/T) - 1}. \tag{3.23}$$

To good approximation we take $h_{\rm eff}(T)$ in $s = 2\pi^2 h_{\rm eff} T^3/45$ to be that of the SM, $h_{\rm eff} = 427/4$. The integrals in (3.23) can be taken exactly, resulting in

$$Y_S = \frac{s}{n_b} \frac{135\zeta(5)}{2\pi^3} \frac{\Gamma_H}{h_{\rm eff} H(m_H)} \simeq 3.8 \times 10^5 \times \frac{A^2 M_P}{m_H^3}, \tag{3.24}$$

where $H(m_H)$ is the value of the Hubble constant at $T = m_H$ and $\zeta(x)$ is the Riemann zeta function.

The decay of the $S$ bosons at late times proceed to muons and hadrons depending on what channels are kinematically allowed. At $m_S \ll 1$ GeV the decay rates can be obtained within the framework of chiral perturbation theory and by low-energy theorems [85,86]. For $m_S \gtrsim 1.5$ GeV or so, perturbative QCD starts getting applicable. Around these energies the decay rate is dominated by $S$ decaying into $s$ quarks with a $\sim$25% contribution to muons:

$$\Gamma_S \simeq \frac{3 m_S}{8\pi} \left( \frac{A m_s \tan\beta}{m_H^2} \right)^2 \left( 1 + \frac{m_\mu^2}{3 m_s^2} \right). \tag{3.25}$$

Notice that heavy-quark-mediated $S \to gg$ decays are suppressed relative to the SM by a factor of 9 because in the large $\tan\beta$ regime only $b$ quarks contribute, and $t$, $c$ contributions are subdominant. Since $m_s \gtrsim m_\mu$, the decays to strange-antistrange pairs happen in at least 75% of the cases. When $m_S$ is below the di-hyperon threshold, each of these decays lead to either $K^-$ or $K_L$ in the final state. The last step in checking the suitability of this model involves trading $A^2$ in the formula for the abundance (3.25) for the lifetime of $S$. Taking $m_s \sim 100$ MeV, we get

$$Y_S = 3.4 \times \left( \frac{10^3 \ \text{sec}}{\tau_X} \right) \left( \frac{2 \ \text{GeV}}{m_S} \right) \left( \frac{m_H \tan^{-2}\beta}{5 \ \text{GeV}} \right), \tag{3.26}$$

where all parameters are normalized on their "natural" values. It is in a way remarkable that in these models many numbers of very different orders of magnitude conspire to yield abundances in the right ballpark necessary for a suppression of the $^7$Li abundance via the emission of kaons (and pions).

## IV. CONCLUSIONS

The current discrepancy between the prediction of the lithium abundance in SBBN and its observation at the Spite-plateau value prompted a number of particle-physics related explanations. Previous works have mainly concentrated on the effects of heavy, electroweak-scale particles on the $^7$Li abundance. Such models typically involve decays of electroweak-scale WIMPs with nucleons among the decay products, or the catalytic suppression of $^7$Li by metastable charged particles, that have their masses again in the electroweak range. In this paper we have considered a related but nevertheless distinct possibility: decays of (sub-)GeV-scale neutral relic particles. Because of their kinematic constraints, neither of these particles can be charged nor can their decay products contain nucleons in the final state. Nevertheless, the reduction of the lithium abundance may occur simply because pions and kaons in the final state have a significant probability of interacting with protons and creating a neutron excess. We have shown that $\mathcal{O}(1) - \mathcal{O}(100)$ abundances of metastable particles with respect to baryons and with lifetimes around a few hundred to ten thousand seconds can easily reduce the lithium abundance by a factor of a few and still be consistent with measurements of primordial deuterium. We have also shown that if the decays to the charged hadrons are kinematically not possible, the muons in the final state can also reduce the overall lithium abundance. In this case the main effect comes from electron antineutrinos that induce $p \to n$ interconversions. It turns out that $\mathcal{O}(10^5)$ muon decays per proton around a few hundred seconds are needed in order to reduce the lithium abundance to observationally favored levels. Moreover, an injection of pions and muons not far from thresholds also leave less "damage" in form of $^6$Li, compared to scenarios with electroweak-mass decaying relics. This is because the $^6$Li production requires significant amounts of energy to split $^4$He and create energetic $A = 3$ nuclei, which in case of the muons/pion injection is far less efficient. This broadens the acceptable lifetime range to up to $O(10^4)$ sec.

We have done a careful numerical investigation of this problem by including charge exchange and absorption reactions of pions, kaons, and (anti)neutrinos on nucleons and $^4$He. In doing so we have updated the values for the most relevant reactions, and integrated them into a Kawano-based nucleosynthesis code. We have also accounted for the change in the neutrino spectrum due to the Hubble expansion and due to neutrino oscillations. The results are presented in the form of abundance-lifetime plots, Figs. 5–8, where we have assumed a maximal branching into each species. We can see that the elevated deuterium abundance is an inevitable consequence of all such scenarios, resulting from the "removal" of extra neutrons by the $np \to d\gamma$ reaction. The only exception is the case of relic particles decaying to muons at $\sim 10^4$ sec. In this case, the late energy injection, combined with early

neutrino-induced $p \to n$ interconversion can lead to the SBBN value of deuterium, and achieve the suppression of $^7$Li by a factor of a few.

In order to relate this proposal to some concrete model realizations, we have considered two minimalistic extensions of the SM. We chose to extend the SM by a singlet scalar $S$ coupled via the so-called Higgs portal, or a new $U(1)_S$ group that has kinetic mixing with the photon field strength. Both models, in principle, possess new long-lived states, and in the case of the $U(1)_S$ model this is either the vector $V$ or the Higgs′ particle $h'$ of the $U(1)_S$-breaking sector. The cosmological history in these models then depends on the strength of the couplings that connect the secluded sectors to the SM particles.

If the couplings to the standard model are large enough, the new GeV-scale states $X$ are thermally excited (WIMP regime). An acceptable abundance of $X = S$, $h'$ prior to decay is then either achieved via annihilation, e.g., $SS \to f\bar{f}$, or via the excitation to the unstable state, $h'e \to Ve \to e\bar{e}e$. We have shown that in the WIMP regime both models provide viable solutions to the lithium problem, and that both, the $\pi$, $K$-mediated or the antineutrino-mediated suppression of $^7$Li indeed work. We have identified the plausible choice for the parameters where such reduction will occur. The same parameters may be chosen to fit the PAMELA and FGST anomalies, when the mediator models are complemented with electroweak-scale WIMPs. In addition to cosmological probes, there is a certain chance of detecting these new GeV-scale states in laboratory experiments, such as in rare decays of mesons, in Higgs decays, and in fixed target experiments. Last but not least, we remark that a $m_{h'} < m_V$ mass pattern naturally arises in straightforward supersymmetric generalizations of the $U(1)_S$ model.

We have further shown that the super-WIMP regime of these models also have a potential to provide a viable resolution to the lithium problem. In this case, the metastable states are never in thermal equilibrium and are only produced via an extremely small thermal rate. Such models are relatively predictive because the mass and the coupling of $X$ can be translated directly into lifetime and abundance predictions. Unfortunately, the extreme smallness of the coupling constants prevents direct experimental searches of such particles in the laboratory. On the other hand, the sensitivity that the early Universe exhibits to new physics is once again emphasized by the fact the lithium and deuterium abundances are capable of probing effective coupling constants as small as $\alpha\kappa^2 \sim 10^{-26}$. It remains to be seen whether the $^7$Li reduction can be achieved in another well-motivated model of super-WIMPs in the form of heavy sterile neutrinos.

To close up, the problem of the $^7$Li abundance definitely deserves special attention, as it hints at one of the very few inconsistencies in the standard cosmological picture. Of course, at this point it is difficult to insist that particle physics must necessarily be key for solving the current lithium problem. Yet, as shown in this paper, several particle-physics scenarios that reduce the $^7$Li abundance are quite natural and perhaps deserve further detailed considerations. As to the lithium problem, only future progress in cosmology, astrophysics, particle, and nuclear physics may help to resolve this intriguing problem.

## ACKNOWLEDGMENTS

Research at the Perimeter Institute is supported in part by the Government of Canada through NSERC and by the Province of Ontario through MEDT. J. P. wants to thank the Galileo Galilei Institute for Theoretical Physics for their hospitality and the INFN for partial support during the final stages of this work.

## APPENDIX

### 1. Some details on the Boltzmann code

The Boltzmann code that we use is based on the one of Ref. [87], in which we incorporate some significant improvements and updates: physical constants, isotope masses, and conversion factors are determined from the evaluations [88,89]. For all important SBBN reactions (i.e. up to $A = 7$) we employ the results of [90] with the exceptions of the $n(p, \gamma)$D and $^3$He$(\alpha, \gamma)^7$Be reactions for which we follow [91,92], respectively. All other $\mathcal{O}(80)$ remaining reactions we update by following the recommendations of [93].

In order to arrive at an accurate prediction of $^4$He we numerically integrate all weak rates at each time step for which zero temperature radiative corrections are taken into account following [94]. When applicable, we further take into account relativistic Coulomb corrections to the weak rates by multiplying the integrands with the Fermi function

$$F(Z, v) = 2(1 + S)(2pR)^{-2(1-S)} \frac{|\Gamma(S + i\eta)|^2}{\Gamma(2S + 2)^2} e^{\pi\eta}, \quad \text{(A1)}$$

where $Z$ is the nuclear charge, $S = (1 - \alpha^2 Z^2)^{1/2}$, $p$ ($v = p/E$) is the momentum (velocity) of the relative motion, and $R \simeq 1$ fm is the proton radius; $\eta$ is given in (A4). In our code we approximate $F(Z, v)$ by [95]

$$\begin{aligned} F(Z, v) &\simeq \sum_{n=0}^{3} a_n (\alpha Z)^n, \quad \text{with } a_0 = 1, \\ a_1 &= \frac{\pi}{v}, \\ a_2 &= \frac{11}{4} - \gamma_E - \ln(2pR) + \frac{\pi^2}{3v^2}, \\ a_3 &= \frac{\pi}{v}\left[\frac{11}{4} - \gamma_E - \ln(2pR)\right], \end{aligned} \quad \text{(A2)}$$

where $\gamma_E \simeq 0.5772$ is the Euler-Mascheroni constant. Note, however, that in the nonrelativistic case, $F(Z, v)$ is better approximated by (A3). As the dividing line we

choose $v = 0.045$ which guarantees that (A2) and (A3) represent (A1) to better than 0.1%. In the nonrelativistic limit the familiar factor reads

$$F(Z, v) \simeq \frac{2\pi\eta}{1 - e^{-2\pi\eta}}, \qquad \eta = \frac{Z\alpha}{v}, \tag{A3}$$

where $Z$ is the nuclear charge; $\eta$ is called the Sommerfeld parameter. Evidently, note that for Coulomb corrections of equally charged particles one has to replace $Z$ by $-Z$, e.g., in $\pi^+ + {}^4\mathrm{He}$ reactions. When obtaining Coulomb corrected cross sections, we make the approximation

$$\langle \sigma v \rangle_i \simeq F(Z, \langle v \rangle)(\sigma v)_i, \qquad \langle v \rangle = \sqrt{2T/\mu}, \tag{A4}$$

where $\mu$ is the reduced mass of the incoming particles.

Finally, as assessed in [94], we apply a slight upward shift of 0.72% of the resulting $^4$He abundance in order to account for more subtle, subleading corrections to the BBN reaction network. We then find very good agreement of our light element abundance predictions with the ones presented in the recent work [3] at the WMAP value of $\eta_b = 6.23 \times 10^{-10}$ and with a neutron lifetime of $\tau_n = 885.7$ sec.

### 2. Pion and kaon capture on helium

Experimental data on absorption of stopped charged mesons on various target materials are usually cast in the form of absorption rates and branching fractions of the reaction fragments. After being stopped, $\pi^-$ are captured into atomic orbits from which they emit X rays (and Auger electrons) until they come close enough to interact strongly with the nucleus. The cascading time is significantly smaller than $\tau_{\pi^\pm}$ and pions reach a $1S$ orbit prior to absorption. A measurement of the ground state level width $\Gamma_{1S} = (45 \pm 3)$ eV [36] of pionic helium then allows us to obtain the low-energy in-flight cross section $(\sigma v)$ of a free $^4$He-$\pi^-$ pair via

$$\Gamma_{1S}^{\mathrm{abs}} = |\psi_{1S}(0)|^2 (\sigma v), \tag{A5}$$

where $|\psi_{1S}(0)|^2 v$ is the flux density at the origin. Assuming a 100% absorption from the $1S$ state, we find for the total $\pi^-$-$^4$He reaction cross section

$$(\sigma^{\pi}_{^4\mathrm{He}} v) \simeq 7.3 \text{ mb}. \tag{A6}$$

To extract the cross sections for the $K^- + {}^4\mathrm{He}$ reaction we can proceed in a similar fashion as for $\pi^- + {}^4\mathrm{He}$. Interestingly, however, measurements of kaonic X rays from $^4$He show no radiative transitions from the $2P \rightarrow 1S$ state [96] which tells us that $K^-$ on the $2P$ level prefers to react strongly with the alpha nucleus rather than undergoing another radiative transition to the ground state. Since $\sim$16% of captured $K^-$ indeed make it to the $2P$ state, this implies a lower bound on the $2P$ absorption rate [96]

$$\Gamma_{2P}^{\mathrm{abs}} \geq 3 \times 10^{14} \text{ sec}^{-1}. \tag{A7}$$

Using that value will, however, only yield the (momentum-dependent) $p$-wave contribution to the total in-flight absorption cross section. Therefore, and since we could not locate further experimental data on $s$-wave absorption, we have to rely on theoretical calculations.

Reference [97] finds for the absorption rate from the $2S$ state $\Gamma_{2S}^{\mathrm{abs}} = 48.1 \times 10^{18}$ sec$^{-1}$ which points towards a very large cross section $(\sigma v) \simeq 1.2$b [using $\psi_{2S}$ instead of $\psi_{1S}$ in (A5)]. This value, however, is in conflict with the $s$-wave unitarity bound $\langle \sigma_{\max} v \rangle \simeq 0.4\mathrm{b}/\sqrt{T_9}$ so that we refrain from using it. We further observe that the quoted value for the $2P$-absorption rate in [97] is a factor of $\sim$20 larger than the experimental lower bound (A7). Employing the (somewhat *ad-hoc*) prescription to scale down $\Gamma_{2S}$ of [97] by the same factor of 20 (which saturates the lower bound for the $2P$-case), we arrive at a total in-flight threshold cross section of

$$(\sigma^{K^-}_{^4\mathrm{He}} v) \simeq 60 \text{ mb}. \tag{A8}$$

Indeed, this cross section compares well with the values inferred from another calculation [98] for $K^-$ absorption from the $1S$ state which gives us some confidence that (A8) lies in the right ballpark.

### 3. Pion reactions across the Delta resonance

The predominant feature in low-energy pion collisons with nucleons and nuclei is the formation of $\Delta$ resonances. For reactions with nucleons, we only need to consider $\pi^- + p \rightarrow \pi^0 + n$ across the resonance. Though at cosmic times $t \lesssim 180$ sec neutrons are still an abundant target, $\pi^+$ are stopped before interacting with them. For the charge-exchange reaction of $\pi^- + p$ we employ the partial-wave analysis of [99,100] as shown in the left panel of Fig. 10 as a function of pion kinetic energy $E_\pi$ in the rest frame of the proton. It agrees well with the experimental results of [101]. The dot at threshold corresponds to (2.26). The alternative exit channel $n + \gamma$ is only relevant at threshold and becomes quickly negligible with increasing pion energy. We have verified this from a model calculation [99,100] of the inverse process of photo-pion production by employing the principle of detailed balance.

The right panel of Fig. 10 shows the various contributions to $\pi^\pm$-$^4$He scattering. The top curve and data "Bin75" represent the total inelastic cross section as taken from [38]. The cross section breaks down into an absorptive part with no pion in the final state and the remaining inelastic part. We fit the in-flight absorption data "Mat98" [40] by scaling down the calculation of [102] by a factor of 0.8; older data "Str90" on absorption is collected in [39]. The dotted parts of the lines show the regions in which we had to extrapolate without data. In particular, note that inelastic pion scattering (without absorption) has thresholds in the range $\sim(15 \div 30)$ MeV depending on the final state. For simplicity, and because absorption dominates for low energies, we have extrapolated the inelastic cross section to a common threshold value $E^{\pi^+}_{4,\mathrm{th}} \sim 25$ MeV.

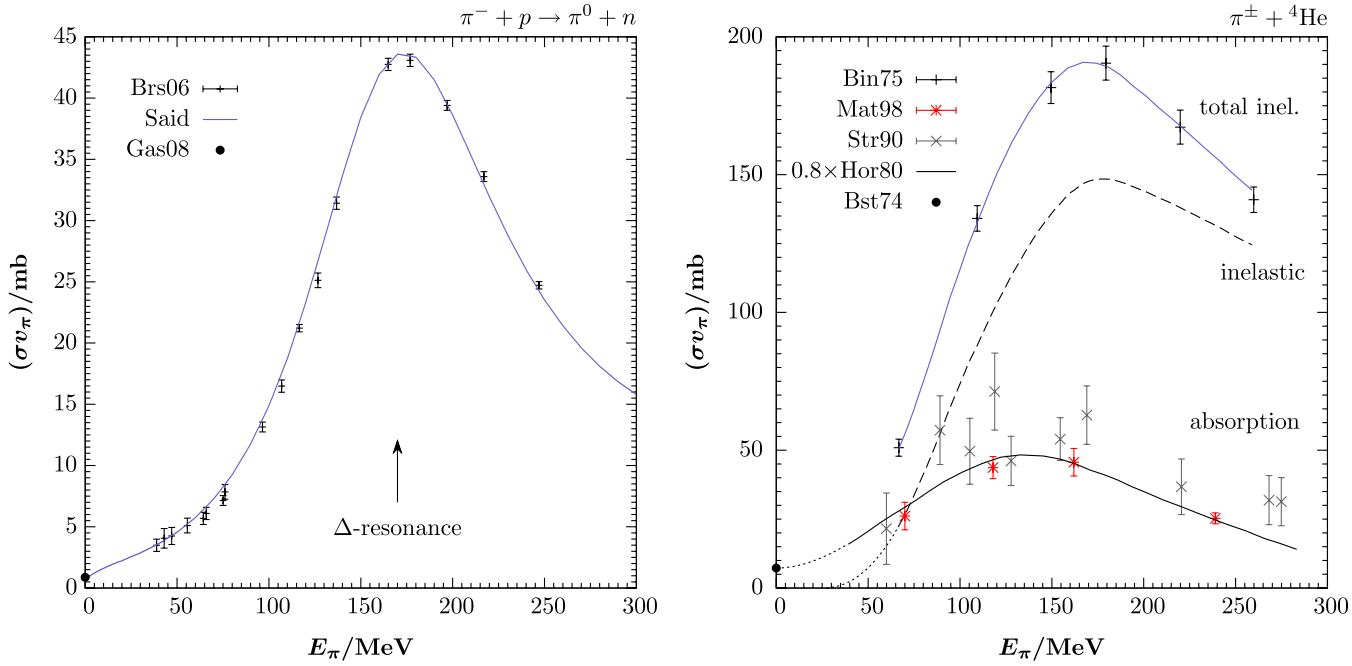


FIG. 10 (color online). Left: Cross section for pion-induced proton conversion, $\pi^- + p \to \pi^0 + n$, across the $\Delta^0$ resonance as a function of pion kinetic energy in the LAB-frame. The solid line shows a pion-nucleon partial-wave model calculation [99,100]. In-flight experimental data labeled Brs06 are from [101], the point at the threshold labeled Gas08 is inferred from the $1S$ level width as quoted in [34]. Right: The top curve shows the total $\pi^\pm$-$^4$He inelastic scattering cross section as given in [38] and labeled as "Bin75." The data labeled Mat98 [40] is the absorptive part; older data Str90 on pion absorption is collected in [39]. We employ the model calculation of [102], scaled by a factor 0.8 to fit Bin75. The dashed line shows the difference between the latter two lines and thus provides the remaining part of the inelastic cross section. The dotted parts of the lines indicate the regions in which we extrapolate without data. The dot at threshold is again inferred from the pionic helium $1S$ level width given in [36].

In particular, the output of $^3$He and T from absorption and inelastic $\pi^\pm$-$^4$He scatterings is important for the non-thermal $^6$Li abundance. The adopted nuclear/nucleon final-state multiplicities are summarized in Table I. For absorption, one finds that the branchings into the various final states differ significantly depending on whether the process occurs at threshold or not. At threshold the fraction of $A = 3$ elements is $\sim$20% but for $E_\pi = 120$ MeV the respective multiplicities, as inferred from the measurements of [39], are already very small. Since, by nature, absorption yields the largest recoil energies such a behavior is not unexpected and between $E_\pi = 0$ and 30 MeV we interpolate between the threshold and in-flight $\xi$ values. For larger pion energies we switch to the in-flight data.

TABLE I. Adopted final-state multiplicities for the various $\pi^\pm$$^4$He reactions. Values are rounded such that the baryon number remains conserved, $3\xi_{^3\mathrm{He}} + 3\xi_\mathrm{T} + 2\xi_\mathrm{D} + \xi_n + \xi_p = 4$.

| process | $\xi_{^3\mathrm{He}}$ | $\xi_\mathrm{T}$ | $\xi_\mathrm{D}$ | $\xi_n$ | $\xi_p$ |
|---|---|---|---|---|---|
| $\pi^+$ absorption, threshold | 0.17 | ⋯ | 0.63 | 0.2 | 2.03 |
| $\pi^-$ absorption, threshold | ⋯ | 0.17 | 0.63 | 2.03 | 0.2 |
| $\pi^+$ absorption, in-flight | 0.01 | ⋯ | 0.1 | 0.87 | 2.9 |
| $\pi^-$ absorption, in-flight | ⋯ | 0.01 | 0.1 | 2.9 | 0.87 |
| $\pi^+$ inelastic, SX | 0.4 | ⋯ | 0.2 | 0.4 | 2.0 |
| $\pi^-$ inelastic, SX | ⋯ | 0.4 | 0.2 | 2.0 | 0.4 |
| $\pi^+$ inelastic, NX | 0.4 | 0.2 | 0.4 | 0.8 | 0.6 |
| $\pi^-$ inelastic, NX | 0.4 | 0.2 | 0.4 | 0.8 | 0.6 |
| $\pi^+$ inelastic, DX | 0 | 0 | 0 | 0 | 4 |
| $\pi^-$ inelastic, DX | 0 | 0 | 0 | 4 | 0 |

Above the threshold of inelastic $\pi^\pm$-$^4$He scattering the energy-dependent multiplicities $\xi_i$ of elements $i = {}^3$He, T, D, $n$, and $p$ are given by

$$\xi^{\pi^\pm}_{i,\mathrm{inel}} = f_\mathrm{SX}\xi^{\pi^\pm}_{i,\mathrm{SX}} + (1 - f_\mathrm{SX})[(1 - g_\mathrm{DX})\xi^{\pi^\pm}_{i,\mathrm{NX}} + g_\mathrm{DX}\xi_{i,\mathrm{DX}}]. \tag{A9}$$

The contribution of a single charge exchange (SX) $f_\mathrm{SX} \equiv \sigma_\mathrm{SX}/\sigma_\mathrm{inel}$ is inferred from the measurements of [103] by simple linear regression, $f_\mathrm{SX} = 0.11 + 6 \times 10^{-4}(E_\pi/\mathrm{MeV})$. We further assume a constant ratio of double charge exchange (DX) to scatterings preserving the incident the pion charge (NX), $g_\mathrm{DX} \equiv \sigma_\mathrm{DX}/\sigma_\mathrm{NX} = 0.1$. For the multiplicities $\xi^{\pi^\pm}_{i,\alpha}$ of the individual processes $\alpha =$ SX, NX, and DX we resort to data of inelastic $^4$He-$p$ scattering. To this end, one observes that for incident beam kinetic energies in excess of $\sim(50 \div 80)$ MeV (above which also pion inelastic scattering starts dominating

over absorpion) the branchings into $^3$He$np$, T2$p$, D$n$2$p$, and DD$p$ become approximately energy independent with respective values $\sim$0.4, 0.2, 0.2, and 0.1 (for moderate energies $\lesssim$ 300 MeV). Adopting those values yield the multiplicities for $^4$He-$\pi^\pm$ reactions as listed in Table I. Note that the $\xi$ values imply a quantitative difference between $\pi^-$-$^4$He and $\pi^+$-$^4$He scattering.

In a similar manner as in Sec. II C where we introduced the correction factor $\kappa$ one can account for the incomplete stopping of pions in reactions on $^4$He by defining an effective cross section for $\pi^{j4}\mathrm{He} \to i$, $i = {}^3$He, T, D, $n$, and $p$, averaged over the pion trajectory,

$$\langle \sigma_{\pi^{j4}\mathrm{He}\to i} v\rangle_{\mathrm{traj.}} = \tau_\pi^{-1} \int_0^\infty dt P_{\mathrm{surv}}(t) F_{\pi^{j4}\mathrm{He}} \times \sum_{\alpha=\mathrm{inel,abs}} (\sigma_{\pi^{\pm 4}\mathrm{He},\alpha} v) \times \xi_{i,\alpha}^{\pi^j} \quad \text{(A10)}$$

where

$$P_{\mathrm{surv}}(t) = \exp\left(-\int_0^t \frac{m_{\pi^\pm}}{\tau_{\pi^\pm}(m_{\pi^\pm} + E_\pi(t'))} dt'\right) \quad \text{(A11)}$$

is the time-dilatated survival probability of the pion. Note that it was not possible to define a correction factor $\kappa$ as in (2.29) because the effective rates for $\pi^{-4}\mathrm{He} \to$ T and $\pi^{+4}\mathrm{He} \to {}^3$He vanish below the threshold of inelastic $\pi^\pm$-$^4$He scattering.

The output of secondary $^6$Li, triggered by $\pi^\pm$-$^4$He reactions and prior to potential destruction on protons, can be tracked via

$$\left.\frac{dn_{^6\mathrm{Li}}}{dt}\right|_{\mathrm{sec}} = n_{^4\mathrm{He}} \sum_{\substack{i={}^3\mathrm{He,T} \\ j=+,-}} \{\langle \Gamma^{\mathrm{inel}}_{\pi^{j4}\mathrm{He}\to i}\rangle * \langle N_{^6\mathrm{Li}}\rangle_{f_i} + \langle \Gamma^{\mathrm{abs}}_{\pi^{j4}\mathrm{He}\to i}\rangle * N_{^6\mathrm{Li}}\}, \quad \text{(A12)}$$

where $\langle \Gamma^{\mathrm{inel/abs}}_{\pi^{j4}\mathrm{He}\to i}\rangle = n_{\pi^j}\langle \sigma^{\mathrm{inel/abs}}_{\pi^{j4}\mathrm{He}\to i} v\rangle_{\mathrm{traj.}}$ are the effective rates for energetic $i = {}^3$He, T production. The dependence of $E_\pi$ on time is suggested by the $*$ in (A12) indicating that the effective rates are to be ''convolved'' with the number of produced secondary $^6$Li per injected $A = 3$ nucleus, $N_{^6\mathrm{Li}}$. For inelastic scattering this involves an additional average over the spectrum $f_i$ of primary mass-3 injection energies $E_{i,\mathrm{in}}$,

$$\langle N_{^6\mathrm{Li}}\rangle_{f_i} = n_{^4\mathrm{He}} \int_{E^i_{6,\mathrm{th}}}^{E_{i,\mathrm{max}}(E_\pi(t))} dE_{i,\mathrm{in}} f_i(E_{i,\mathrm{in}}, E_\pi(t)) \times \int_{E_{i,\mathrm{in}}}^{E^i_{6,\mathrm{th}}} dE_i \frac{(\sigma_{i+^4\mathrm{He}\to{}^6\mathrm{Li}+X} v_i)}{dE_i/dt}, \quad \text{(A13)}$$

where we employ [14]

$$f_i(E_{i,\mathrm{in}}, E_\pi) = \mathcal{N}^{-1} \sum_{k=1,2} w_{i,k} E_{i,\mathrm{in}}^{1/2} e^{-E_{i,\mathrm{in}}/T_k} \times \left(\frac{E_{i,\mathrm{max}} - E_{i,\mathrm{in}}}{E_{i,\mathrm{max}}}\right). \quad \text{(A14)}$$

Note that we have introduced a kinematical cutoff in the last factor; $E_{i,\mathrm{max}}(E_\pi)$ is the maximal kinetic recoil energy of $A = 3$ in the rest frame of the mother $^4$He nucleus (which approximately coincides with the frame of the thermal bath) and can be found by simple kinematical considerations (see also below). The spectra (A14) are obtained from fits to experimental $p$-$^4$He data with coefficients $(w_{^3\mathrm{He}}) = (1, 0.19)$, $(T_{^3\mathrm{He}}/\mathrm{MeV}) = (1.9, 4.9)$ and $(w_{\mathrm{T}}) = (1, 0.15)$, $(T_{\mathrm{T}}/\mathrm{MeV}) = (1.3, 3.9)$ [104,105]. The normalization factor $\mathcal{N}$ is chosen such that $\int_0^{E_{i,\mathrm{max}}} dE_{i,\mathrm{in}} f_i = 1$.

Finally, we remark that for pion absorption, the resulting nonthermal $^6$Li yield is easier to track because T and $^3$He are injected monoenergetically in the CM frame so that $\langle N_{^6\mathrm{Li}}\rangle_{f_i} \to N_{^6\mathrm{Li}}$ as in (2.36). The primary $A = 3$ injection energy in the rest frame of $^4$He (the frame of the thermal bath) then depends on the scattering angle and lies within the interval

$$E_{3,in}(E_\pi) \in \frac{1}{2m_3}\left[\pm\sqrt{2\mu'\left(\frac{\mu_{\pi 4}}{m_{\pi^\pm}} E_\pi + Q\right)} + \frac{\sqrt{2m_{\pi^\pm} E_\pi} m_3}{m_{\pi^\pm} + m_\alpha}\right]^2, \quad \text{(A15)}$$

where $\mu_{\pi 4}$ and $\mu'$ are the respective reduced masses before and after scattering. In our code, we adopt the central value. Figure 11 shows the efficiency for the production of a secondary $^6$Li nucleus, per injected $^3$He + T as a function of temperature. Pion absorption (solid and dotted lines) *a priori* is the most efficient way of generating $^6$Li as the $A = 3$ recoil is maximized. The probabilities have to be weighted by the mass-3 multiplicities and relative strengths of absorption and inelastic scattering. Moreover, it has to be stressed that Fig. 11 does not include $^6$Li destruction on thermal protons which ultimately determines the surviving lithium fraction.

### 4. Electromagnetic energy injection

Our treatment of the nonthermal electromagnetic component introduced in the decay of pions, kaons, and muons is mainly along the lines of Ref. [106]. The injection of energetic primaries $e^\pm$ and/or $\gamma$ particles leads to a quick formation of an electromagnetic cascade via the processes of inverse Compton scattering and $e^\pm$-pair production on background photons. The resulting ''zeroth-generation'' differential photon spectrum is given by a broken power law [107],

$$p_\gamma(E_\gamma) = \begin{cases} K_0(E_\gamma/E_{\mathrm{low}})^{-1.5} & \text{for } E_\gamma < E_{\mathrm{low}} \\ K_0(E_\gamma/E_{\mathrm{low}})^{-2.0} & \text{for } E_{\mathrm{low}} < E_\gamma < E_C \\ 0 & \text{for } E_\gamma > E_C \end{cases}, \quad \text{(A16)}$$

with a cutoff at the pair-production threshold $E_C \simeq m_e^2/22\mathrm{T}$ and a power break at $E_{\mathrm{low}} \simeq m_e^2/(80\ \mathrm{T})$ [42].

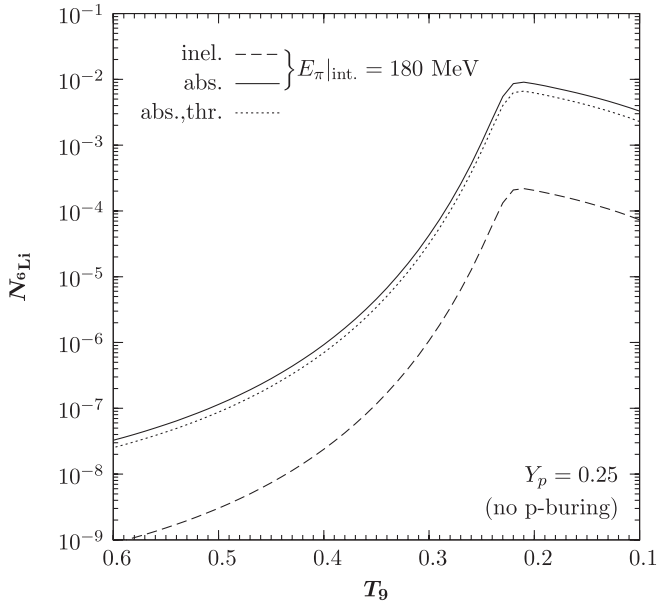


FIG. 11. Number of secondary $^6$Li produced per injected $^3$He + T prior to potential destruction on protons. The dotted line shows $N_{^6\rm Li}$ for absorption on the threshold [compare (2.36)]. The solid and dashed lines show the probability of producing $^6$Li from in-flight reactions of a pion with fixed kinetic energy $E_\pi|_{\rm int.} = 180$ MeV on $^4$He via absorption and inelastic scattering, respectively. For the latter compare with (A13). These curves have to be convoluted with the actual energy-dependent branching into mass-3 elements as in (A12). Note that $p$ burning will have a substantial effect on the ultimately surviving fraction of secondary $^6$Li down to the lowest temperatures shown.

The overall normalization of the spectrum is determined from the primary injected energy $E_0$,

$$E_0 = \int dE_\gamma E_\gamma p_\gamma(E_\gamma) = K_0 E_{\rm low}^2 (2 + \ln(E_C/E_{\rm low}). \quad \text{(A17)}$$

The photons in the cascade (A16) undergo further degradation via the (slower) processes of Compton scattering, pair-production on nuclei, and elastic $\gamma$-$\gamma$ scattering so that the total number of energetic photons is given by a competition of injection rate $\Gamma_{\rm inj}$ and total energy-loss rate $\Gamma_\gamma(E_\gamma)$. The energy spectrum can then be obtained in form of a quasistatic equilibrium solution

$$f_\gamma^{\rm qse} = n_X \frac{\Gamma_{\rm inj} p_\gamma(E_\gamma)}{\Gamma_\gamma(E_\gamma)}, \quad \text{(A18)}$$

where $n_X$ is the time-dependent number density of the decaying particles, and $\Gamma_{\rm inj} = \tau_X^{-1}$. For the thermalization rate we put

$$\Gamma_\gamma = \Gamma_{\rm BH,p} + \Gamma_{\rm BH,^4He} + k(E_\gamma)\Gamma_C + 0.5\Gamma_{\gamma\gamma}, \quad \text{(A19)}$$

where $\Gamma_{\rm BH,N}$, $\Gamma_C$, and $\Gamma_{\gamma\gamma}$ are the respective rates for Bethe-Heitler scattering, Compton scattering, and $\gamma$-$\gamma$ scattering. For $\Gamma_{{\rm BH},N} = n_N \sigma_{{\rm BH},N}$ we employ the cross-section formulas as given in [42]. The rate for Compton scattering, $\Gamma_C = n_e \sigma_{\rm KN}$, depends on the Klein-Nishina cross section $\sigma_{\rm KN}$ [108] and on the total electron (positron) number density $n_e$, with an average fractional energy loss per scattering [107],

$$k(E_\gamma) \simeq 1 - \frac{4/3}{\ln(2E_\gamma/m_e) + 1/2}. \quad \text{(A20)}$$

The rate of photon scattering on blackbody photons, obtained in [109], reads

$$\Gamma_{\gamma\gamma}(E_\gamma) = \frac{2^5 139 \pi^4 \alpha^4}{3^6 5^4} \frac{m_e}{2\pi} \left(\frac{T}{m_e}\right)^6 \left(\frac{E_\gamma}{m_e}\right)^3, \quad \text{(A21)}$$

and is valid below the $e^\pm$ pair-production threshold. The factor of 1/2 in (A19) can be understood by noting that photon-photon scattering tends to split primary gamma rays into two gamma rays carrying on average each 50% of the primary energy [109]. Taken all together, $\Gamma_\gamma^{-1}$ then defines an approximate survival time for the "zeroth-generation" photons.

The production and destruction of elements due to electromagentic energy injection can then be described by the Boltzmann equations for nuclei $T$, $A$, $P$, $(A_T > A_A > A_P)$:

$$-HT\frac{dY_A}{dT} = \sum_T Y_T \int_0^\infty dE_\gamma f_\gamma^{\rm qse}(E_\gamma) \sigma_{\gamma+T\to A}(E_\gamma) - Y_A \sum_P \int_0^\infty dE_\gamma f_\gamma^{\rm qse}(E_\gamma) \sigma_{\gamma+A\to P}(E_\gamma). \quad \text{(A22)}$$

In our Boltzmann code we include all processes determined in [106] from which we also take the photodissociation cross sections $\sigma_{\gamma+i\to j}$. Finally, we remark that we also take into account the secondary production of $^6$Li by fusion reactions of energetic mass-3 elements which are produced by photo spallations of $^4$He. The efficiency of producing $^6$Li can be found in analogy to (2.36).

[1] J. Dunkley *et al.*, Astrophys. J. Suppl. Ser. **180**, 306 (2009).
[2] F. Iocco, G. Mangano, G. Miele, O. Pisanti, and P. D. Serpico, Phys. Rep. **472**, 1 (2009).
[3] R. H. Cyburt, B. D. Fields, and K. A. Olive, J. Cosmol. Astropart. Phys. 11 (2008) 012.
[4] G. Steigman, Annu. Rev. Nucl. Part. Sci. **57**, 463 (2007).

[5] K. Jedamzik and M. Pospelov, New J. Phys. **11**, 105028 (2009).
[6] F. Spite and M. Spite, Astron. Astrophys. **115**, 357 (1982).
[7] M. H. Reno and D. Seckel, Phys. Rev. D **37**, 3441 (1988).
[8] K. Jedamzik, Phys. Rev. D **70**, 063524 (2004).
[9] M. Kawasaki, K. Kohri, and T. Moroi, Phys. Lett. B **625**, 7 (2005).
[10] M. Kawasaki, K. Kohri, and T. Moroi, Phys. Rev. D **71**, 083502 (2005).
[11] K. Jedamzik, Phys. Rev. D **74**, 103509 (2006).
[12] F. D. Steffen, J. Cosmol. Astropart. Phys. 09 (2006) 001.
[13] R. H. Cyburt, J. R. Ellis, B. D. Fields, K. A. Olive, and V. C. Spanos, J. Cosmol. Astropart. Phys. 11 (2006) 014.
[14] R. H. Cyburt *et al.*, J. Cosmol. Astropart. Phys. 10 (2009) 021.
[15] A. Freitas, F. D. Steffen, N. Tajuddin, and D. Wyler, Phys. Lett. B **682**, 193 (2009).
[16] K. Jedamzik, Phys. Rev. D **70**, 083510 (2004).
[17] K. Jedamzik, K.-Y. Choi, L. Roszkowski, and R. Ruiz de Austri, J. Cosmol. Astropart. Phys. 07 (2006) 007.
[18] D. Cumberbatch *et al.*, Phys. Rev. D **76**, 123005 (2007).
[19] M. Pospelov, Phys. Rev. Lett. **98**, 231301 (2007).
[20] C. Bird, K. Koopmans, and M. Pospelov, Phys. Rev. D **78**, 083010 (2008).
[21] T. Jittoh *et al.*, Phys. Rev. D **76**, 125023 (2007).
[22] M. Kusakabe, T. Kajino, R. N. Boyd, T. Yoshida, and G. J. Mathews, arXiv:0711.3858.
[23] N. Arkani-Hamed, D. P. Finkbeiner, T. R. Slatyer, and N. Weiner, Phys. Rev. D **79**, 015014 (2009).
[24] M. Pospelov and A. Ritz, Phys. Lett. B **671**, 391 (2009).
[25] O. Adriani *et al.* (PAMELA Collaboration), Nature (London) **458**, 607 (2009).
[26] A. A. Abdo *et al.* (Fermi LAT Collaboration), Phys. Rev. Lett. **102**, 181101 (2009).
[27] M. Pospelov, A. Ritz, and M. B. Voloshin, Phys. Lett. B **662**, 53 (2008).
[28] J. L. Feng, M. Kaplinghat, and H.-B. Yu, arXiv:1005.4678.
[29] M. Cirelli and J. M. Cline, arXiv:1005.1779.
[30] P. J. Fox and E. Poppitz, Phys. Rev. D **79**, 083528 (2009).
[31] Y. Nomura and J. Thaler, Phys. Rev. D **79**, 075008 (2009).
[32] B. Batell, M. Pospelov, and A. Ritz, Phys. Rev. D **80**, 095024 (2009).
[33] C. Amsler *et al.* (Particle Data Group Collaboration), Phys. Lett. B **667**, 1 (2008).
[34] J. Gasser, V. E. Lyubovitskij, and A. Rusetsky, Phys. Rep. **456**, 167 (2008).
[35] T. Flugel, Report No DISS-ETH-13105 (unpublished).
[36] G. Backenstoss, J. Egger, T. von Egidy, R. Hagelberg, C. J. Herrlander, H. Koch, H. P. Povel, A. Schwitter, and L. Tauscher, Nucl. Phys. **A232**, 519 (1974).
[37] E. Daum, S. Vinzelberg, D. Gotta, H. Ullrich, G. Backenstoss, P. Weber, H. J. Weyer, M. Furic, and T. Petkovic, Nucl. Phys. **A589**, 553 (1995).
[38] F. G. Binon and *et al.* (Brussels-Orsay Collaboration), Phys. Rev. Lett. **35**, 145 (1975).
[39] M. Steinacher, G. Backenstoss, M. Izycki, P. Salvisberg, P. Weber, H. J. Weyer, A. Hoffart, B. Rzehorz, H. Ullrich, M. Dzemidzic, M. Furic, and T. Petkovic, Nucl. Phys. **A517**, 413 (1990).
[40] A. O. Mateos *et al.* (LADS Collaboration), Phys. Rev. C **58**, 942 (1998).
[41] S. Dimopoulos, R. Esmailzadeh, L. J. Hall, and G. D. Starkman, Nucl. Phys. **B311**, 699 (1989).
[42] M. Kawasaki and T. Moroi, Astrophys. J. **452**, 506 (1995).
[43] P. Bonifacio, L. Pasquini, F. Spite, A. Bragaglia, E. Carretta, V. Castellani, M. Centuriòn, A. Chieffi, R. Claudi, G. Clementini, F. D'Antona, S. Desidera, P. François, R. G. Gratton, F. Grundahl, G. James, S. Lucatello, C. Sneden, and O. Straniero, A&A International **390**, 91 (2002).
[44] J. Melendez and I. Ramirez, Astrophys. J. **615**, L33 (2004).
[45] W. Aoki *et al.*, Astrophys. J. **698**, 1803 (2009).
[46] L. Sbordone, P. Bonifacio, E. Caffau, H. Ludwig, N. T. Behara, J. I. Gonzalez Hernandez, M. Steffen, R. Cayrel, B. Freytag, C. Van't Veer, P. Molaro, B. Plez, T. Sivarani, M. Spite, F. Spite, T. C. Beers, N. Christlieb, P. Francois, and V. Hill, arXiv:1003.4510.
[47] J. Melendez, L. Casagrande, I. Ramirez, M. Asplund, and W. Schuster, arXiv:1005.2944.
[48] S. Burles and D. Tytler, Astrophys. J. **507**, 732 (1998).
[49] D. Kirkman, D. Tytler, N. Suzuki, J. M. O'Meara, and D. Lubin, Astrophys. J. Suppl. Ser. **149**, 1 (2003).
[50] Y. I. Izotov and T. X. Thuan, Astrophys. J. **710**, L67 (2010).
[51] E. Aver, K. A. Olive, and E. D. Skillman, arXiv:1001.5218.
[52] M. Asplund, D. L. Lambert, P. E. Nissen, F. Primas, and V. V. Smith, Astrophys. J. **644**, 229 (2006).
[53] M. Steffen, R. Cayrel, P. Bonifacio, H. G. Ludwig, and E. Caffau, arXiv:1001.3274.
[54] *Origin and Evolution of the Elements: Proceedings of a symposium in honour of H. Reeves, held in Paris, June 22-25, 1992*, edited by N. Prantzos, E. Vangioni-Flam, and M. Casse (Cambridge University Press, Cambridge, 1993).
[55] R. H. Dalitz and S. F. Tuan, Ann. Phys. (N.Y.) **10**, 307 (1960).
[56] A. D. Martin and G. G. Ross, Nucl. Phys. **B16**, 479 (1970).
[57] P. A. Katz, K. Bunnell, M. Derrick, T. Fields, L. G. Hyman, and G. Keyes, Phys. Rev. D **1**, 1267 (1970).
[58] T. Kanzaki, M. Kawasaki, K. Kohri, and T. Moroi, Phys. Rev. D **75**, 025011 (2007).
[59] R. J. Scherrer, Mon. Not. R. Astron. Soc. **210**, 359 (1984).
[60] G. G. Raffelt, *Stars as Laboratories for Fundamental Physics: The Astrophysics of Neutrinos, Axions, and Other Weakly Interacting Particles.* (University of Chicago Press, Chicago, 1996), p 664.
[61] S. Pastor, G. G. Raffelt, and D. V. Semikoz, Phys. Rev. D **65**, 053011 (2002).
[62] C. Bemporad, G. Gratta, and P. Vogel, Rev. Mod. Phys. **74**, 297 (2002).
[63] A. Strumia and F. Vissani, Phys. Lett. B **564**, 42 (2003).
[64] T. Yoshida, T. Suzuki, S. Chiba, T. Kajino, H. Yokomakura, K. Kimura, A. Takamura, and D. H. Hartmann, Astrophys. J. **686**, 448 (2008).
[65] D. P. Finkbeiner and N. Weiner, Phys. Rev. D **76**, 083519 (2007).
[66] J. McDonald, Phys. Rev. D **50**, 3637 (1994).
[67] C. P. Burgess, M. Pospelov, and T. ter Veldhuis, Nucl. Phys. **B619**, 709 (2001).
[68] J. McDonald, Phys. Rev. Lett. **88**, 091304 (2002).
[69] B. Holdom, Phys. Lett. B **166**, 196 (1986).

[70] M. Pospelov, Phys. Rev. D **80**, 095002 (2009).
[71] B. Batell, M. Pospelov, and A. Ritz, arXiv:0911.4938.
[72] C. Bird, P. Jackson, R. V. Kowalewski, and M. Pospelov, Phys. Rev. Lett. **93**, 201803 (2004).
[73] C. Bird, R. V. Kowalewski, and M. Pospelov, Mod. Phys. Lett. A **21**, 457 (2006).
[74] A. Badin and A. A. Petrov, arXiv:1005.1277.
[75] B. Batell, M. Pospelov, and A. Ritz, Phys. Rev. D **79**, 115008 (2009).
[76] M. Reece and L.-T. Wang, J. High Energy Phys. 07 (2009) 051.
[77] R. Essig, P. Schuster, and N. Toro, Phys. Rev. D **80**, 015003 (2009).
[78] M. Baumgart, C. Cheung, J. T. Ruderman, L.-T. Wang, and I. Yavin, J. High Energy Phys. 04 (2009) 014.
[79] J. D. Bjorken, R. Essig, P. Schuster, and N. Toro, Phys. Rev. D **80**, 075018 (2009).
[80] B. Batell, M. Pospelov, A. Ritz, and Y. Shang, Phys. Rev. D **81**, 075004 (2010).
[81] P. Schuster, N. Toro, and I. Yavin, Phys. Rev. D **81**, 016002 (2010).
[82] I. Z. Rothstein, T. Schwetz, and J. Zupan, J. Cosmol. Astropart. Phys. 07 (2009) 018.
[83] F. Chen, J. M. Cline, and A. R. Frey, Phys. Rev. D **80**, 083516 (2009).
[84] J. Redondo and M. Postma, J. Cosmol. Astropart. Phys. 02 (2009) 005.
[85] M. B. Voloshin, Sov. J. Nucl. Phys. **44**, 478 (1986).
[86] T. N. Truong and R. S. Willey, Phys. Rev. D **40**, 3635 (1989).
[87] L. Kawano, Report No. FERMILAB-PUB-92-004-A.
[88] G. Audi, A. H. Wapstra, and C. Thibault, Nucl. Phys. **A729**, 337 (2003).
[89] P. J. Mohr and B. N. Taylor, Rev. Mod. Phys. **77**, 1 (2005).
[90] P. Descouvemont, A. Adahchour, C. Angulo, A. Coc, and E. Vangioni-Flam, arXiv:astro-ph/0407101.
[91] S. Ando, R. H. Cyburt, S. W. Hong, and C. H. Hyun, Phys. Rev. C **74**, 025809 (2006).
[92] R. H. Cyburt and B. Davids, Phys. Rev. C **78**, 064614 (2008).
[93] R. H. Cyburt, A. M. Amthor, R. Ferguson, Z. Meisel, K. Smith, S. Warren, A. Heger, R. D. Hoffman, T. Rauscher, A. Sakharuk, H. Schatz, F. K. Thielemann, and M. Wiescher, Astrophys. J. Suppl. Ser. **189**, 240 (2010).
[94] R. E. Lopez and M. S. Turner, Phys. Rev. D **59**, 103502 (1999).
[95] D. H. Wilkinson, Nucl. Phys. **A377**, 474 (1982).
[96] C. E. Wiegand and R. H. Pehl, Phys. Rev. Lett. **27**, 1410 (1971).
[97] T. Onaga, H. Narumi, and T. Kohmura, Prog. Theor. Phys. **82**, 222 (1989).
[98] A. K. Common and K. Higgins, Nucl. Phys. **60**, 465 (1964).
[99] R. A. Arndt, I. I. Strakovsky, and R. L. Workman, Int. J. Mod. Phys. A **18**, 449 (2003).
[100] A. Bellaachia *et al.*, *NSTAR 2002 Workshop on the Physics of Excited Nucleons, Pittsburgh, Pennsylvania, 2002*, edited by S. A. Dytman and E. S. Swanson (World Scientific Publishing, Singapore, 2003) .
[101] J. Breitschopf *et al.*, Phys. Lett. B **639**, 424 (2006).
[102] Y. Horikawa, M. Thies, and F. Lenz, Nucl. Phys. **A345**, 386 (1980).
[103] A. Lehmann, D. Androić, G. Backenstoss, D. Bosnar, T. Dooling, M. Furić, P. A. M. Gram, N. K. Gregory, A. Hoffart, C. H. Q. Ingram, A. Klein, K. Koch, J. Köhler, B. Kotliński, M. Kroedel, G. Kyle, A. O. Mateos, K. Michaelian, T. Petković, M. Planinić, R. P. Redwine, D. Rowntree, N. Šimičević R. Trezeciak, H. Ullrich, H. J. Weyer, and M. Wildi, Phys. Rev. C **60**, 024603 (1999).
[104] A. V. Blinov and M. V. Chadeeva, Phys. At. Nucl. **69**, 1439 (2006).
[105] A. V. Blinov and M. V. Chadeeva, Phys. Part. Nucl. **39**, 526 (2008).
[106] R. H. Cyburt, J. R. Ellis, B. D. Fields, and K. A. Olive, Phys. Rev. D **67**, 103521 (2003).
[107] R. J. Protheroe, T. Stanev, and V. S. Berezinsky, Phys. Rev. D **51**, 4134 (1995).
[108] J. M. Jauch and F. Rohrlich, *Texts and Monographs in Physics* (Springer, New York, 1976), 2nd ed..
[109] R. Svensson and A. Zdziarski, Astrophys. J. **349**, 415 (1990).